Czech Technical University in Prague
Faculty of Electrical Engineering
Department of Cybernetics

Master's thesis

Measurement of tissue optical properties

Bc. Martin Hlaváč

Supervisor: RNDr. Martin Michl, Ph.D.

9th May 2013

Czech Technical University in Prague
Faculty of Electrical Engineering

Department of Cybernetics

DIPLOMA THESIS ASSIGNMENT

Student: Bc. Martin H l a v á č

Study programme: Biomedical Engineering and Informatics

Specialisation: Biomedical Engineering

Title of Diploma Thesis: Measurement of Tissue Optical Properties

Guidelines:

1. Perform a bibliography search on the topic and familiarize yourself with the terms related.
2. Analyze methods for determining tissue optical properties and summarize advantages and disadvantages of individual methods.
3. Develop a new method based on spatially resolved diffuse reflectance measurement.
4. Verify suggested method on data obtained from Monte Carlo simulation.
5. Perform an experiment and verify the method on tissue simulating phantoms.

Bibliography/Sources:

[1] Boas, D. A.; Pitris, C.; Ramanujam, N.: Handbook of biomedical optics / edited by David A. Boas, Constantinos Pitris, Nimmi Ramanujam. Boca Raton, FL : CRC Press, c2011., 2011, ISBN 1420090372.

[2] Grossweiner, L. I.; Rogers, B. H. G.; Grossweiner, J. B.; etc.: The Science of Phototherapy: An Introduction / by Leonard I. Grossweiner, James B. Grossweiner, B.H. Gerald Rogers ; edited by Linda R. Jones. Dordrecht : Springer, 2005., 2005, ISBN 9781402028854.

[3] Tuchin, V. V.: Tissue optics: light scattering methods and instruments for medical diagnosis / Valery Tuchin. SPIE Press monograph: PM166, Bellingham, Wash. : SPIE/International Society for Optical Engineering, c2007., 2007, ISBN 9780819464330.

[4] Welch, A. J.; Gemert, M. J.: Optical-Thermal Response of Laser-Irradiated Tissue / edited by Ashley J. Welch, Martin J.C. Gemert. Dordrecht : Springer Science+Business Media B.V., 2011., 2011, ISBN 9789048188314

Diploma Thesis Supervisor: RNDr. Martin Michl, Ph.D.

Valid until: the end of the summer semester of academic year 2013/2014

prof. Ing. Vladimír Mařík, DrSc.
Head of Department

ČESKÉ VYSOKÉ UČENÍ TECHNICKÉ V PRAZE Fakulta elektrotechnická
L.S.

prof. Ing. Pavel Ripka, CSc.
Dean

Prague, January 10, 2013

České vysoké učení technické v Praze
Fakulta elektrotechnická

Katedra kybernetiky

ZADÁNÍ DIPLOMOVÉ PRÁCE

Student: Bc. Martin H l a v á č

Studijní program: Biomedicínské inženýrství a informatika (magisterský)

Obor: Biomedicínské inženýrství

Název tématu: Měření optických vlastností tkáně

Pokyny pro vypracování:

1. Proveďte rešerši na téma práce a seznamte se s pojmy týkajícími se tématu.
2. Prozkoumejte možné metody na měření optických vlastností tkáně a uveďte výhody a nevýhody jednotlivých metod.
3. Navrhněte novou metodu založenou na měření prostorově rozlišené difúzní reflektance.
4. Ověřte navrženou metodu na datech z Monte Carlo simulace.
5. Proveďte experiment a ověřte platnost metody na tkáňových fantomech.

Seznam odborné literatury:

[1] Boas, D. A.; Pitris, C.; Ramanujam, N.: Handbook of biomedical optics / edited by David A. Boas, Constantinos Pitris, Nimmi Ramanujam. Boca Raton, FL : CRC Press, c2011., 2011, ISBN 1420090372.

[2] Grossweiner, L. I.; Rogers, B. H. G.; Grossweiner, J. B.; etc.: The Science of Phototherapy: An Introduction / by Leonard I. Grossweiner, James B. Grossweiner, B.H. Gerald Rogers ; edited by Linda R. Jones. Dordrecht : Springer, 2005., 2005, ISBN 9781402028854.

[3] Tuchin, V. V.: Tissue optics: light scattering methods and instruments for medical diagnosis / Valery Tuchin. SPIE Press monograph: PM166, Bellingham, Wash. : SPIE/International Society for Optical Engineering, c2007., 2007, ISBN 9780819464330.

[4] Welch, A. J.; Gemert, M. J.: Optical-Thermal Response of Laser-Irradiated Tissue / edited by Ashley J. Welch, Martin J.C. Gemert. Dordrecht : Springer Science+Business Media B.V., 2011., 2011, ISBN 9789048188314

Vedoucí diplomové práce: RNDr. Martin Michl, Ph.D.

Platnost zadání: do konce letního semestru 2013/2014

prof. Ing. Vladimír Mařík, DrSc.
vedoucí katedry

L.S.

prof. Ing. Pavel Ripka, CSc.
děkan

V Praze dne 10. 1. 2013

Acknowledgements

This thesis would not have been possible unless great attitude and support of my supervisor. *RNDr. Martin Michl, Ph.D.* enables me working at external university and always was helpful during writing and organizations. I cannot find words to express my gratitude to him.

I wish to express my sincere gratitude also to *Dr. Liu, Quan Ph.D.* for a great opportunity to work in his team. His guidance was always very helpful in working on this thesis.

Finally my great thanks go to my friend, PhD. student *Zhu, Caigang* for a great assistance with all problems and especially the time he gave me. I really appreciate his guiding at laboratory work.

My thanks include also my friends and family for support during writing this thesis.

Declaration

I hereby declare that I have completed this thesis independently and that I have listed all the literature and publications used in accordance with Methodical directive for adhering ethical principle during academical final theses elaboration.

In Prague 9th May 2013

Czech Technical University in Prague
Faculty of Electrical Engineering

Citation of this thesis

Martin Hlaváč. *Measurement of tissue optical properties: Master's thesis.* Czech Republic: Czech Technical University in Prague, Faculty of Electrical Engineering, 2013.

Abstract

Knowledge of the optical properties is in medicine very important for modeling of light propagation in tissue, diagnosis and therapeutical methods. The aim of a theoretical part is understanding of tissue optics and different approaches for determining optical properties in a turbid medium such as tissue. In experimental part we are designing a new method for determining optical properties - absorption coefficient μ_a and reduced scattering coefficient μ_s'. This method represents a fast, non-invasive and device minimalistic approach of measurement in small volumes. We focus on spatially resolved measurement of diffuse reflectance and using an empirical model.

Keywords tissue optics, spatially resolved diffuse reflectance, tissue optical properties, tissue phantoms, turbid medium

Abstrakt

Znalost optických vlastností tkáně je v medicíně velmi důležitá pro modelování průchodu světla tkání, diagnózu a terapeutické metody. Cílem teoretické část této práce je seznámení s tkáňovou optikou obecně a různými přístupy pro měření optických vlastností v turbidním médiu, jakým je tkáň. V experimentální části se zabýváme návrhem nové metody měření optických vlastností jako je absorpční koeficient μ_a a redukovaný difúzní koeficient μ_s'. Tato metoda zajišťuje rychlý, neinvazivní a přístrojově nenáročný způsob měření v malých objemech. Zaměřili jsme se na prostorově rozlišené měření difúzní odrazivosti a použití empirického modelu.

Klíčová slova tkáňová optika, prostorově rozlišená difúzní odrazivost, optické vlastnosti tkáně, tkáňové fantomy, turbidní médium

Contents

List of Figures

List of Tables

Introduction

Optical methods in medicine are mostly used for diagnostic and therapeutic application. The diagnostic methods include for example early cancer detection, optical imaging, monitoring of blood oxygenation and tissue metabolism. Laser surgery together with photodynamic therapy belong to mainly used therapeutic methods [4, 5]. Nowadays, the measurement of the tissue optical properties remains one of the main tasks of biomedical optics [41]. The advancing progress in biophotonics requires improvement of the measurement techniques [5].

In theoretical part of this thesis, the principle of tissue optic and the basic light interactions with the turbid medium are described. Absorption and elastic scattering are prevalent phenomena and they are important for modeling light propagation in turbid medium. Various models are introduced and methods (both direct and indirect) for optical properties determination are described. While direct methods are based on basic principles, indirect methods use one of the light propagation models for solving inverse problem and determination of the optical properties.

With these knowledge, a new method of measurement is suggested. Our requirements are speed, cost-effective equipment and non-complicated model. According to the worldwide trend, our method is based on diffuse reflectance measurement. We prefer spatially resolved measurement before spectrally constrained, time resolved and frequency domain. It is advantageous due to low-cost equipment and possibility of using non-complicated model. The suggested method is also suitable for measurement in very small volumes what makes it advantageous for endoscopy or measuring tissue inhomogeneity.

Our method is firstly validated on data from Monte Carlo simulation and results are processed in Matlab®. Further, measurement on tissue simulating phantoms is performed. Due to their well defined optical properties, the phantoms are ideal for method development and validation and their preparation is described in this thesis as well.

CHAPTER 1

Tissue optic

Progress in science and technology in the past decades brings along a new possibilities in medicine. Biomedical optics has still increasing number of applications in therapeutic and diagnostic techniques. And hence well described light propagation in biological materials is the main task of tissue optic. This includes determination of the optical properties as absorption and scattering. With this knowledge we can find the light energy delivered to the required area (for example in photodynamic therapy) [64]. Altogether this forms the theoretical basis about tissue optic.

Despite progression in tissue optic the real-time analysis of optical properties still remains a problem. There are different reasons why single methods are limited. Ideal method should ensure real-time, noninvasive and accurate measurement. This method would be also possible in very small samples or areas and hence would be able to measure tissue inhomogeneity. Our method is developed on these bases.

1.1 Fundamental theory

Biological tissue is turbid, inhomogeneous optical medium with refractive index higher than air. Therefore part of light is reflected on the air/tissue interface. Typical values for tissue is 1.35 - 1.45 [71]. Turbid medium is described as medium both with absorbing and scattering properties [21, 60]. Photons in such medium move in all directions and may be scattered or absorbed. Tissue is also characterized by huge diversity and structural complexity. Size of tissue structure varies from tenthes nanometers to hundreds micrometers. The most important optical properties for description of light propagation are absorption coefficient and scattering coefficient (eventually reduced scattering coefficient, as will be written later). Knowledge of these coefficients

is very important in both therapeutic and diagnostic applications of light in medicine [35].

1.2 Tissue optical properties

Optical properties are determined mostly in so-called therapeutic (or diagnostic) window with wavelength between 600 and 1600 nm in the visible and near infrared region. Because of low absorption of the tissue light can achieve deep penetration $(8 - 10\ mm)$[60]. In this region prevails scattering over absorption. Spectral regions are described in detail in Table 1.1.

Region	**Wavelength range** $[nm]$	**Photon energy range** $[eV]$
UV-C	$\sim 100 - 280$	$\sim 12.4 - 4.4$
UV-B	$\sim 280 - 320$	$\sim 4.4 - 3.9$
UV-A	$\sim 320 - 400$	$\sim 3.9 - 3.1$
Visible	$\sim 400 - 800$	$\sim 3.1 - 1.55$
Near-IR	$\sim 800 - 1200$	$\sim 1.55 - 1.03$
Middle-IR	$\sim 1200 - 7000$	$\sim 1.03 - 0.18$
Far-IR	$\sim 7000 - 1000000$	$\sim 0.18 - 0.0012$

Table 1.1: Division of electromagnetic spectrum between UV and IR region with corresponding wavelength and energy [64].

Description of absorption is relatively simple, the absorbed photon does not continue further and its path ends there. If the photon is absorbed, there are several possibility of reaction with the tissue [21]. But for description of scattering we need to know the direction of photon after scattering event. This information carries scattering phase function $p(\theta)$. Phase function specifies the angular distribution of scattering by a single scattering center. The phase function can be also represented by the mean cosine of the scattering angle g, which can be combined with the scattering coefficient to give the reduced (or transport) scattering coefficient. Most of scattering events are elastic and wavelength is not changed during the light propagation in the tissue [21]. Very important is also fact, that absorption coefficient and scattering coefficient varies with different wavelength [20]. That is used in spectrally-constrained diffuse reflectance measurement. There are more optical properties than described here, but they are just derived from these fundamental ones. They will be described in Section 1.2.3. Summary of all parameters is in Table 1.2.

1.2.1 Absorption

Absorption phenomena is responsible for light attenuation in the tissue. Photon transmits his energy to the molecules and it cause excitation of the molecular electronic, vibrational or rotational states. The interaction is dependent on

MICROSCOPIC PARAMETERS	
FUNDAMENTAL	
μ_a	Absorption coefficient $[mm^{-1}]$
μ_s	Scattering coefficient $[mm^{-1}]$
$p(\theta)$	Scattering phase function
DEPENDENT	
μ_t	Total attenuation coefficient $[mm^{-1}]$
$1/\mu_t$	Penetration depth $[mm]$ (mean free path)
a	Albedo: $a = \mu_s/\mu_t$
g	Anisotropy coefficient
τ	Optical thickness: $\tau = d(\mu_a + \mu_s)$, d...physical thickness
μ_s'	Reduced scattering coefficient $[mm^{-1}]$
a'	Reduced albedo $a' = \mu_s'/(\mu_a + \mu_s')$
MACROSCOPIC PARAMETERS	
μ_{eff}	Effective attenuation coefficient $[mm^{-1}]$
δ_{eff}	Effective penetration depth $1/\mu_{eff}$ [mm]
R_t	Total reflectance: $R_d = R_s + R_d$
R_s	Specular reflectance
R_d	Diffuse reflectance
T_t	Total transmittance: $T_t = T_c + T_d$
T_c	Colimated transmittance (unscattered)
T_d	Diffuse transmittance

Table 1.2: Microscopic and macroscopic parameters of the tissue [9, 16, 48, 64, 65]

the wavelength of the incident light, type of the tissue and chromophores in the tissue[1]. We are interested in the region of therapeutic window. It is due to high absorption of hemoglobin in UV region and high absorption of water in IR region [8]. Absorption is described by Lambert-Beer law:

$$I = I_0 e^{-\mu_a s} \ , \tag{1.1}$$

where s is the travel distance of the light in the medium and μ_s is absorption coefficient. I_0 is the light intensity at $s = 0$ and I is light intensity attenuated by absorption. Absorption coefficient describes how far can photon penetrate into tissue before being absorbed. It can be also understand in the meaning

[1] chromophore are compounds responsible for the absorption [68]

of probability distribution function [64].

$$P_a(S < s) = F_a(s) = 1 - e^{-\mu_a s} \tag{1.2}$$

Equation 1.2 represents probability of absorption event in distance S smaller than distance s. Inverse value of absorption coefficient $1/\mu_a$ is called mean free path for absorption event [21]. Absorption can be also described by particle density ρ:

$$\mu_a = \rho\sigma_a \ , \tag{1.3}$$

where σ_a is absorption cross section:

$$\sigma_a = q_a A_a \ , \tag{1.4}$$

where q_a is absorption efficiency and A_a geometrical cross section for absorption element. Graphical definition of the absorption cross section is in Figure 1.1.

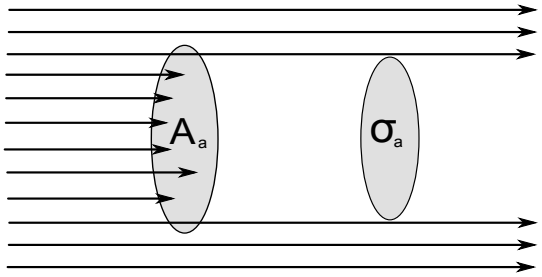

Figure 1.1: Absorption cross section

Typical values of absorption coefficient are between 0.5 cm^{-1} and 5 cm^{-1} in the VIS and IR region [60].

1.2.1.1 Absorption spectra for the main chromophores

Absorption coefficient of the tissue can be determined with the knowledge of the single chromophores. Using volume concentration and molar extinction coefficient ϵ of each chromophore we can calculate total absorption coefficient:

$$\mu_a = \sum_i c_i(\mathbf{r}, t) \cdot \epsilon_i(\lambda) \ , \tag{1.5}$$

where $c_i(\mathbf{r}, t)$ is the chromophore concentration at position $\mathbf{r}$ in time t. Extinction coefficient describes effectiveness of a compound as an absorber (also called specific absorbance) [68].

Water is among the most important chromophores because tissue contains approximately 75% of it. Absorption spectrum of water is shown in

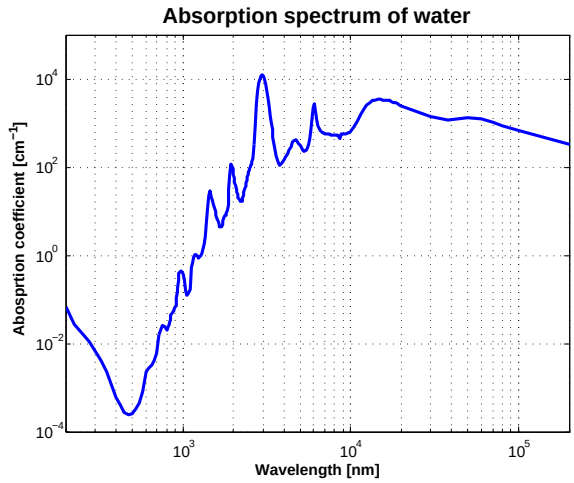

Figure 1.2: Absorption spectrum of water between $200nm$ and $200\mu m$

Figure 1.2. It shows that water is significant chromopher in the NIR regime. Absorption spectrum was measured by Hale and Querry [22].

Hemoglobin is next important absorber. Absorption spectrum of human hemoglobin was reviewed and collected by Prahl [53], Figure 1.3. Hemoglobin in oxygenated state is called oxyhemoglobin and in reduced state deoxyhemoglobin. Their spectra deviates and that is used for measuring blood oxygenation. Absorption coefficient of the hemoglobin in Figure 1.3 is calculated for blood with concentration 150 $g/liter$.

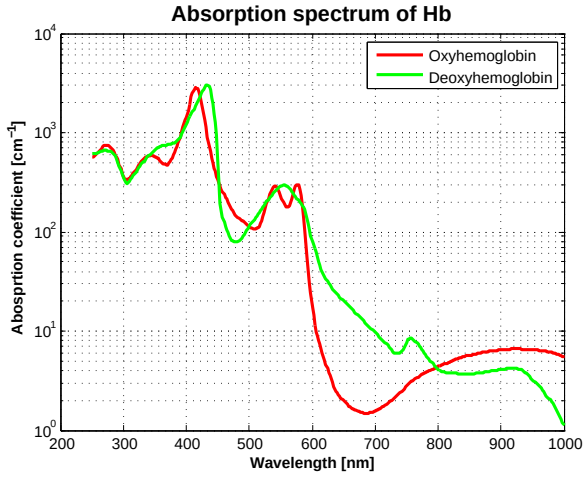

Figure 1.3: Absorption spectrum of hemoglobin between 200 and $1000nm$

Lipids spectrum was obtained from pork fat [62]. In NIR region the amplitude is in the similar order as water.

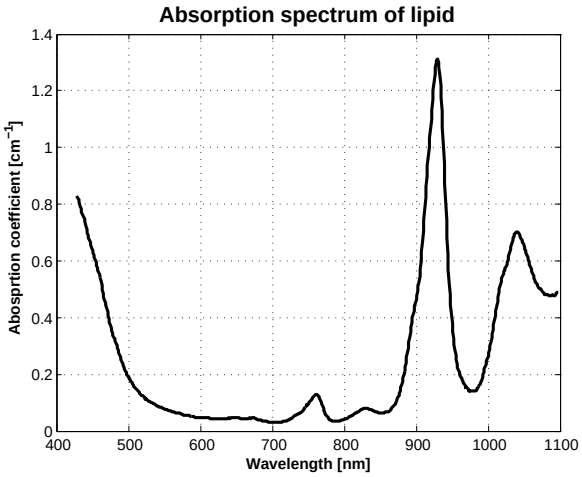

Figure 1.4: Absorption spectrum of lipids

Others proteins and amino acids are important absorbers in UV and lower part of VIS regime. For example melanin is used as protection against UV radiation and hence is important absorber in this region [12].

1.2.2 Scattering

Scattering is dominant mechanism in the tissue in NIR region and prevails over absorption. Photons will be scattered even in very thin layer of the tissue [20]. Due to the interaction with a scatterer the direction of the photon is changed and after several numbers of scattering events light loses its initial directionality. Scattering is mainly caused by changes in refractive index on the microscopical level. Refractive index mismatch on the macroscopic level is mostly ignored in methods described in Chapter 2. Scattering can be divided into elastic and inelastic. Inelastic scattering such as Raman scattering is characterized by change of the wavelength of the incident photon. In the range of VIS and NIR region scattering is mainly elastic and therefore scattered photon continues with the same wavelength after scattering event. Scattering is also dependent on the wavelength and usually decreases with the increasing wavelength (although for the blood there is an exception) [64]. Scattering was firstly described by Rayleigh in 1871 [21] and his theory still can be used for description scattering on the particles much smaller than wavelength. Later was introduced Mie theory (1908) derived for the scattering by spherical particles of any size [2].

[2]Mie theory for the small particles can be approximated by Rayleigh's theory

We will describe scattering coefficient analogically to the absorption coefficient. The scattering coefficient μ_s [mm^{-1}, cm^{-1}] describes probability of scattering for each photon.

$$P_s(S < s) = F_s(s) = 1 - e^{-\mu_s s} \tag{1.6}$$

Inverse value of scattering coefficient $1/\mu_s$ is called mean free path for scattering event [21]. Scattering can be also described by particle density:

$$\mu_s = \rho\sigma_s \ . \tag{1.7}$$

Scattering cross section is graphically illustrated in Figure 1.5 and calculation is adequate as absorption cross section:

$$\sigma_s = q_s A_s \ , \tag{1.8}$$

where q_s is scattering efficiency and A_s geometrical cross section for scattering element.

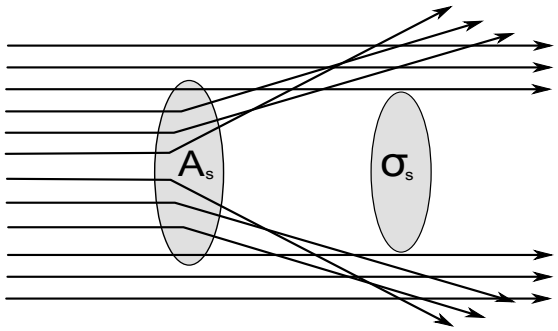

Figure 1.5: Scattering cross section

And using Lambert-Beer law in the same form as absorption coefficient:

$$I = I_0 e^{-\mu_s s}. \tag{1.9}$$

But for complete description of scattering event we need to describe single scattering phase function. It is due to the spatially dependence of continuing photons. This function is denoted as $p(\hat{\mathbf{s}}, \hat{\mathbf{s}}')$, where direction of the incident photon is described by vector $\hat{\mathbf{s}}'$ and direction of the scattered photon by $\hat{\mathbf{s}}$ [4, 20]. Although tissue is anisotropic, we can assume that the scattering depends only on the angle between vectors $\hat{\mathbf{s}}$ and $\hat{\mathbf{s}}'$ [64]. We denote this angle as θ and phase function can be rewritten as:

$$p(\hat{\mathbf{s}}', \hat{\mathbf{s}}) = p(\theta) \tag{1.10}$$

Phase function can be represented by anisotropy factor g - mean cosine of the scattering angle.

$$g =< cos\theta >= \int_{-1}^{1} p(cos\theta) cos\theta \, \mathrm{d}(cos\theta) \tag{1.11}$$

For total forwards scattering $g = 1$ and for total reverse scattering $g = -1$. For isotropic scattering $g = 0$ (but inverse is not always true) [5, 64]. The scattering is mainly forward directed in the tissue. Typically values of g for biological tissue are: $0.7 < g < 0.9$ [21], which corresponds to the angle from 25° to 45°. For Monte Carlo simulations and in transport equation has been used several phase functions [64]. Mostly are used:

- Henyey-Greenstein phase function:

$$p_{HG} = p(\hat{\mathbf{s}}', \hat{\mathbf{s}}) = \frac{1}{4\pi} \frac{1 - g^2}{(1 + g^2 - 2gcos\theta)^{3/2}}. \tag{1.12}$$

  Experimentally it has been shown it is a good approximation, although it does not exactly represent the true phase function of biological tissue. Mainly because higher moments are determined from the first one: $g_l = g_1^l$ [26]. This function approximate the angular dependence of Mie Scattering [21, 64].

- Modified Henyey-Greenstein phase function:

$$p_{HG_m} = p(\hat{\mathbf{s}}', \hat{\mathbf{s}}) = \frac{1}{2\pi} \frac{1}{2} \left[\beta + (1 - \beta) \frac{1 - g^2}{(1 + g^2 - 2gcos\theta)^{3/2}} \right]. \tag{1.13}$$

  It includes isotropic component - β represents isotropically scattered fraction of light.

- Linear Anisotropic phase function:

$$p_{LA} = p(\hat{\mathbf{s}}', \hat{\mathbf{s}}) = \frac{1}{2\pi} \frac{1}{2} (1 + 3gcos\theta). \tag{1.14}$$

- δ-Eddington approximation:

$$p_{\delta-E} = p(\hat{\mathbf{s}}', \hat{\mathbf{s}}) = \frac{1}{2\pi} \frac{1}{2} \left[2f\delta(1 - cos\theta) + (1 - f)(1 + 3gcos\theta) \right], \tag{1.15}$$

  where f represents the fraction of photons scattered in the direction $\hat{\mathbf{s}}'$ and $f =< 0, 1 >$.

Because diffusion theory assumes isotropic scattering (and in the tissue the scattering is mainly forward directed) a new coefficient is used. Using similarity principle we can assume medium with anisotropic scattering to be medium

with isotropic scattering with the condition of long travel distance within the tissue [66]. By combining anisotropy and scattering coefficient we obtain *reduced scattering coefficient (or transport scattering coefficient).*

$$\mu_s' = \mu_s(1-g) \tag{1.16}$$

Reduced scattering coefficient can be defined as inverse distance between effectively scattering events, where photon loses all memory of its initial direction [50]. This combined coefficient is very often used in measurement tissue optical properties and is fundamental parameter in diffusion theory. Typical value of scattering coefficient is between 0.2 cm^{-1} and 400 cm^{-1}. For $g = 0.9$ it gives us reduced scattering coefficient between 0.02 cm^{-1} and 40 cm^{-1} [60].

1.2.3 Dependent optical properties

The most important coefficient measured in biological tissue are absorption coefficient μ_a and reduced scattering coefficient μ_s'. But there are more coefficients used for the tissue description. First is the total attenuation coefficient, μ_t can be written as the sum of μ_a and μ_s:

$$\mu_t = \mu_a + \mu_s. \tag{1.17}$$

From μ_t is derived penetration depth $1/\mu_t$, also called MFP (mean free path). Analogically reduced (or transport) total attenuation coefficient μ_t' is described:

$$\mu_t' = \mu_a + \mu_s'. \tag{1.18}$$

Another parameter is the effective attenuation coefficient:

$$\mu_{eff} = (3\mu_a(\mu_a + \mu_s'))^{3/2}, \tag{1.19}$$

which describes the exponential attenuation of light in the tissue. Next parameter often used in integrating sphere measurement is optical thickness [48]:

$$\tau = d(\mu_s + \mu_a), \tag{1.20}$$

where d is physical thickness of the slab. This parameters are used in various models and remains important for description light propagation.

1.3 Light propagation in the tissue

To summarize previous text, light in the tissue can be absorbed or scattered. Scattered light can return back towards the source or it is transmitted through the tissue or phantom [64] (with neglected reflection on the surface). The basic interactions are shown in Figure 1.6. It is the simplest conception of photons moving in the turbid medium. Problem of description light propagation can be

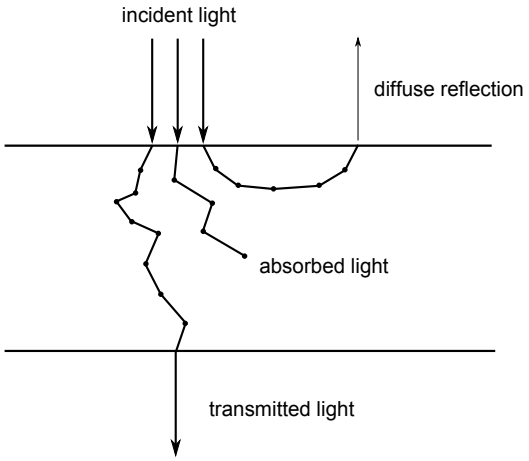

Figure 1.6: Light propagation in the turbid medium.

solved either analytically or using transport theory. Analytic solution starts with Maxwell equation and transport theory calculate directly with the transport of energy in turbid medium. Basically electromagnetic theory describes light propagation by superposition of electromagnetic fields, transport theory uses energy fluxes [12]. Therefore transport theory can neglect phenomena typical for the electromagnetic theory as polarization, interference and phase.

First we need to define optical parameters used in transport theory and description of light propagation in the turbid medium [64].

Radiance $L(\mathbf{r},\hat{\mathbf{s}})$

Radiance describes propagation of photon energy, the unit is $[W \cdot m^{-2} \cdot sr]$. Exact definition of radiance is: "at a point of a surface and in a given direction, the radiant intensity of an element of the surface, divided by the area of the orthogonal projection of this element on a plane perpendicular to the given direction" [64]. In mathematic term radiance is defined as:

$$L(\mathbf{r},\hat{\mathbf{s}}) = N(\mathbf{r},\hat{\mathbf{s}})c_t, \tag{1.21}$$

where c_t is speed of light in tissue.

Photon density $N_0(\mathbf{r})$**, Angular photon density** $N(\mathbf{r},\hat{\mathbf{s}})$

Photon density is defined as number of photons per unit volume. Angular photon density is defined as a number of photons per unit volume moving in the direction of unit vector $\hat{\mathbf{s}}$ within solid angel $\mathrm{d}\omega$. We can obtain photon density as integral of angular photon density over all directions:

$$N_0(\mathbf{r}) = \int_{4\pi} N(\mathbf{r},\hat{\mathbf{s}})\mathrm{d}\omega \tag{1.22}$$

Fluence rate $\phi(\mathbf{r})$

It is defined as: "the number of photons traveling per unit time per unit area (perpendicular to the direction of propagation) over all directions" [59]. Fluence rate can be obtained by integrating radiance over all solid angles [11]:

$$\phi(\mathbf{r}) = \int_{4\pi} L(\mathbf{r},\hat{\mathbf{s}})\mathrm{d}\omega \tag{1.23}$$

Unit of fluence rate is $[W \cdot m^{-2}]$. In tissue optics it has more practical significance than the radiance. It is because tissue contains absorbing chromophores and they can absorb photons irrespective of their initial direction [64].

Net flux vector $F(\mathbf{r})$

Flux describes photon energy transport per unit area [64]. Vector sum of elemental flux vectors $L(\mathbf{r},\hat{\mathbf{s}})\hat{\mathbf{s}}$ is defined as net flux vector $[W \cdot m^{-2}]$:

$$F(\mathbf{r}) = \int_{4\pi} L(\mathbf{r},\hat{\mathbf{s}})\hat{\mathbf{s}}\mathrm{d}\omega \tag{1.24}$$

Irradiance E $[W \cdot m^{-2}]$

Its definition is: "radiant power incident on an infinitesimal surface element containing the point of interest divided by the area of that element" [25]. Radiant power $P[W]$ is defined as: "power emitted, transferred or received as irradiation" [64].

Terms like radiance, fluence rate and flux are described in term of photon propagation [64]. But we can expand definitions to describe radiant energy by introducing a factor $h\nu$: h is Planck's constant, ν is frequency and $h\nu[J]$ gives photon energy. [59].

Transport theory or radiative transfer theory was originally introduced by Arthur Schuster in 1903 [27]. Transport equation (equivalent to Boltzmann equation) is derived from RTT. Equation 1.25 gives together optical properties such as absorption coefficient, scattering coefficient and scattering phase function. Photon flux is described in the terms of radiance L [60].

$$\frac{\partial L(\mathbf{r},\hat{\mathbf{s}})}{\partial s} = -\mu_t L(\mathbf{r},\hat{\mathbf{s}}) + \frac{\mu_s}{4\pi}\int_{4\pi} L(\mathbf{r},\hat{\mathbf{s}})p(\hat{\mathbf{s}},\hat{\mathbf{s}}')\mathrm{d}\Omega' \tag{1.25}$$

- L($\mathbf{r}$,$\hat{\mathbf{s}}$)- radiance, $\mathbf{r}$, $[W/m^2 \cdot st]$
- $\mu_t = \mu_a + \mu_s$ - total attenuation coefficient, [1/mm]
- $p(\hat{\mathbf{s}},\hat{\mathbf{s}}')$ - scattering phase function, [1/sr]
- $d\Omega'$ - unit solid angle about direction $\hat{\mathbf{s}}'$, $[sr]$

The transport equation expresses changes of the radiance at position $\mathbf{r}$ in direction $\hat{\mathbf{s}}$ due to loses caused by absorption and scattering. There is assumed no radiation source inside the medium [5]. Analytical solution exists only for very simple geometries and solution useful for biomedical applications has still not been demonstrated. Therefore some approximation or probabilistic method has to by used. Forward modeling of light propagation in the tissue is mainly described in two ways: diffusion approximation to the radiative transfer theory or Monte Carlo simulation [13]. Another approach is Kubelka-Munk multiflux theory [33] or discretization adding doubling method [12, 14]. We will describe these approaches for modeling light propagation in the tissue. Several assumption are made for the modeling: scattering and absorbing centers are uniformly distributed in the medium and tissue is assumed to be semi-infinite medium in most methods. That is insufficient for modeling in multilayered medium and hence more complicated model are used.

1.3.1 Diffusion theory

Diffusion approximation is an approximate solution to the transport equation. It is derived by expansion Equation 1.25 in spherical harmonics. Derivation from transport equation is straightforward but lengthy. Light propagation is here described by diffusion fluxes and photon migration is modeled as a diffusion of energy driven by gradient in the material [12]. Time-independent diffusion equation was derived in the form [18]:

$$\nabla^2\phi(\mathbf{r}) - \frac{\mu_a}{D}\phi(\mathbf{r}) = \frac{S(\mathbf{r})}{D} \tag{1.26}$$

where $D = [3(\mu_a + \mu_s')]^{-1}$ is diffusion constant and $S(\mathbf{r})$ is source term. Diffusion equation has its limitations. It is valid only for material where scattering is dominant[3]. The mean free path of the medium has to be much smaller than distance of detection area from the source. This is mainly problematic for use with endoscopic probe, where very short source-detector separation is needed. Scattering and anisotropy coefficient are also combined into the reduced scattering coefficient. Equation 1.26 was determined for steady state measurement and time dependent diffusion equation requires an additional term describing increasing or decreasing flux density [21, 43]:

$$-\frac{1}{c_t D}\cdot\frac{\partial\phi(\mathbf{r},t)}{\partial t} + \nabla^2\phi(\mathbf{r},t) - \frac{\mu_a}{D}\phi(\mathbf{r},t) = \frac{S(\mathbf{r},t)}{D}\ , \tag{1.27}$$

where c_t is speed of light in the medium. Diffusion equation is relatively simple but for determining optical properties we need to characterize the light source and satisfy boundary conditions [18]. There are several variants to the diffusion approximation, for example δ-P1 approximation [24] or P3 approximation [26]. P1 approximation is equivalent to the diffusion approximation,

[3] for NIR regime tissue is such a material

but δ-P1 approximation is modified by adding collimated contributions to the phase function and radiance approximation. Very often used diffusion model was described by Farrell *et al.* [18]. Nowadays lot of methods are using this article as a starting point and is frequently cited.

1.3.2 Kubelka-Munk and multi-flux model

In multi-flux methods the interior flux is divided into two or more streams moving in different directions. The basic Kubelka-Munk two flux model is modeling light incidence on the slab using two counter propagating fluxes. Slab is irradiated by diffuse incidence flux in this model and it is divided in forward stream and backward stream. Forward stream is decreased by absorption and scattering events and increased by backward scattering of opposite stream (for second stream it is applicable in the same manner). It was derived for plane parallel layer with matched boundaries. This model was further developed and evolved in "multi-flux" models. Three-flux model is used with additional collimated incident beam. In four-flux model it is extend by forward and backward collimated fluxes (the irradiance is collimated) [68]. Six-fluxes and seven-fluxes models were designed by adding more fluxes in different directions. This theories are related to the transport equation by parameters A_{KM} (sometime also K_{KM}) and S_{KM}. It is difficult to relate them directly to the transport equation and there are several different methods. Summarization of the methods was made by Cheong *et al.* [9] . We will introduce one for medium where scattering is dominant:

$$\begin{aligned} A_{KM} &= S_{KM}(a-1);\ S_{KM} = \ln\left[\frac{1-R_d(a-b)}{T_t}\right] \\ a &= \frac{1-T_t^2+R_d^2}{2R_d};\ b=\sqrt{a^2-1} \\ A_{KM} &= 2\mu_a;\ S_{KM} = \frac{3}{4}\mu_s(1-g)-\frac{1}{4}\mu_a \\ T_c &= exp(-\mu_t d),\ d...sample\ thickness. \end{aligned} \tag{1.28}$$

In Equations 1.28 the Kubelka-Munk theory is related to the radiative transfer theory. From measured values of collimated transmittance T_c, diffuse reflectance R_d and total transmittance T_t we can obtain all three parameters (μ_s, μ_a, g) [5]. Multi-flux approach remains useful for absorbing layers, where assumptions for diffusion theory and for diffuse incident illumination are not fulfilled . On the other hand diffusion approximation is more accurate than multi-flux theory [21].

1.3.3 Monte Carlo simulation

The probabilistic method Monte Carlo is often used for modeling light propagation in the biological tissue. Monte Carlo method for this purpose was firstly

used in 1983 by Adams and Wilson with isotropic scattering. Anisotropic scattering was introduced a few years later [64]. Monte Carlo method is based on probabilistic models and tracing photons trajectory. In the simulation

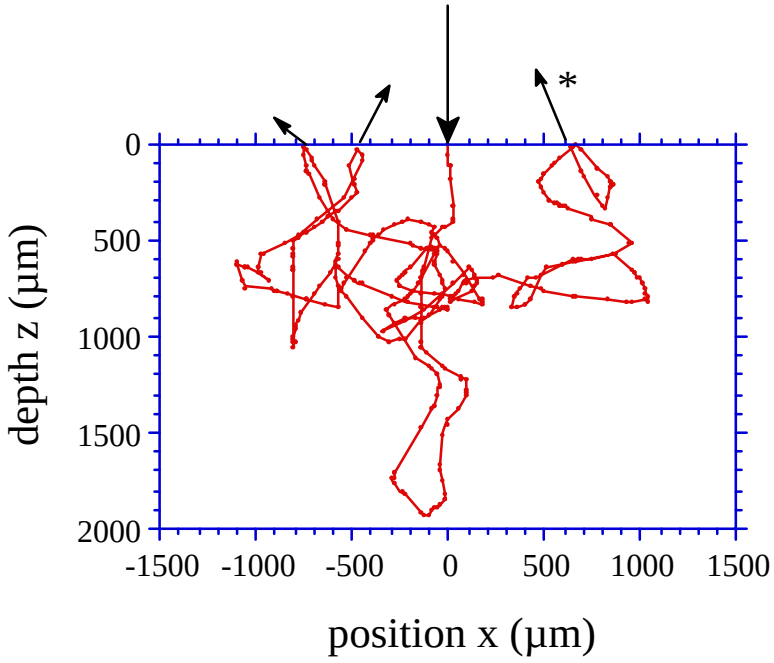

Figure 1.7: Movement of photons in the homogeneous medium - Monte Carlo simulation. *Figure taken from: [63]*

the photons are initialized with coordinates (x, y, z), angles (θ, ϕ) and initial weight $W = W_0$. Initial coordinates depends on the source characteristic and position. Then the trajectory is calculated using step size s:

$$s = -\ln \frac{\xi}{\mu_t}, \tag{1.29}$$

where $\xi = (0, 1)$ is random variable. Photon movement is determined using phase function and at each step photon loses his weight according to the absorption coefficient:

$$W_{new} = W(1 - a), \tag{1.30}$$

where W is weight before a single step and a is albedo. If photon reaches the boundaries, weight is changed according to the Fresnel equation and addition to the transmittance (on the rear boundaries) or reflectance (on the front boundaries) is calculated. If $W < W_{limit}$[4] than the photon walk can be terminated but not in every case. When photon weight falls bellow minimal value,

[4] W_{limit} is usually 10^{-4} [64]

algorithm employs so-called roulette routine: the random number is generated between 0 and 1 and if it is smaller than threshold (usually 0.1), photon continues in his trajectory with recalculated weight $W = W + threshold$ [5]. Actual flux density in the medium is calculated as the superposition of many thousands of photon paths [21]. It has several advantages against diffusion theory, because it often fails close to the source or boundaries and in tissues where scattering is compared to absorption [64]. The mismatched boundaries and loses at the edges can be also taken in account. It can be modeled with any phase function and for both multi-layered model and semi-infinite medium model. Even change in the local optical properties can be included [64]. But because it is probabilistic method the number of traced photons needs to be very high and calculation time rises. A few improvements to accelerate the calculations was introduced [42], [45]. Standard deviation can be calculated as $1/\sqrt{N}$, where N is number of launched photons. Also time-resolved and frequency-domain Monte Carlo method can be implemented [64].

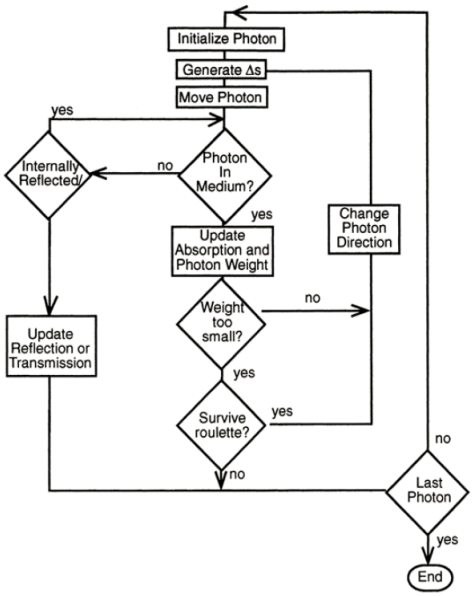

Figure 1.8: Flowchart of Monte Carlo simulation. *Figure taken from: [21]*

1.3.4 Adding-doubling

Adding-doubling method can be used for general, numerical solution of radiative transfer equation. Original algorithm of doubling method was introduced by H. C. van de Hulst in 1962 [48]. Knowledge of one layer transmission $T(\nu, \nu')$ and reflection $R(\nu, \nu')$ for a thin homogeneous layer for incident light at angle ν and exiting at an angle ν' is important for this method. Then by juxtaposing two identical thin layers we can obtain reflection and transmission

for layer twice as thick assuming the contribution from each layer. By repeating this approach we can calculate transmission and reflection for arbitrary thick layer. Method is applicable for any albedo, optical thickness or phase function. The adding methods extends these method for a layer with different optical properties. It can be used for multi-layer models or to simulate internal reflection. Similarly we can implement boundary condition by adding a new layer. Advantage of this method is high accuracy and with longer calculation time it can be very precise. Physical interpretation is available at each step and this method is equivalent for both isotropic and anisotropic scattering. For calculations it requires only integration over angle. Disadvantage of this method is complicated calculation of internal fluences (but it is not a problem for optical properties determination because we can use only transmission and reflection), it is suited to a layered geometry with uniform irradiation and each layer need to have homogeneous optical properties. These last two conditions need to be fulfilled by sample geometry and adequate illumination [2].

1.4 Typical values of tissue optical properties

Tissue optical properties were already measured countless time for various types of tissue. There is summarization of the typical values for different types of the tissue in Appendix B . It is only examples to illustrate the range of the optical properties. A comprehensive summary can be found in literature [5].

CHAPTER 2

Basic principles of tissue optical properties measurement

Number of methods based on the principles discussed in the first chapter were used for tissue optical properties determination . Most of them is using integrating sphere and diffuse reflectance measurement like frequency domain, time domain and spatially resolved steady-state. There are several advantages and disadvantages specific for each method [41].

2.1 Methods categorization

In general we can categorize methods of optical properties determination by several ways.

- Photometric x Photothermal
  - this division is not usually used because photometric methods are dominantly used
  - photothermal methods include for example PPTR - pulsed photothermal radiometry or PAS - photoacoustic spectroscopy [64]
- Ex vivo x In vivo
  - ex vivo methods are accurate and are also suitable for direct methods
  - in vivo is category which we are interested in and further we will be focusing on this methods

- Direct x Indirect
  - ex vivo are further divided into these two categories
  - direct methods are very simple and allow measurement of tissue optical properties directly
  - indirect methods are using inverse model for optical properties determination

We need to distinguish different method of measurement from method of calculation (or algorithms of determination). For example we can measure diffuse reflectance and if we are measuring in vivo we can use several models to determine optical properties. Diffusion approximation and Monte Carlo methods are among the mostly used. We will discuss all models and algorithms in each section.

2.2 Ex-vivo methods

Dominant mechanism of the measurement in this category is integrating sphere measurement. Both single-sphere (Fig. 2.1, 2.3(b,c,d)) and double-sphere (Fig. 2.2) can be used. Double-integrating sphere is preferable for simultaneous measurement of reflectance and transmittance. That leads to smaller sample degradation during the measurement.

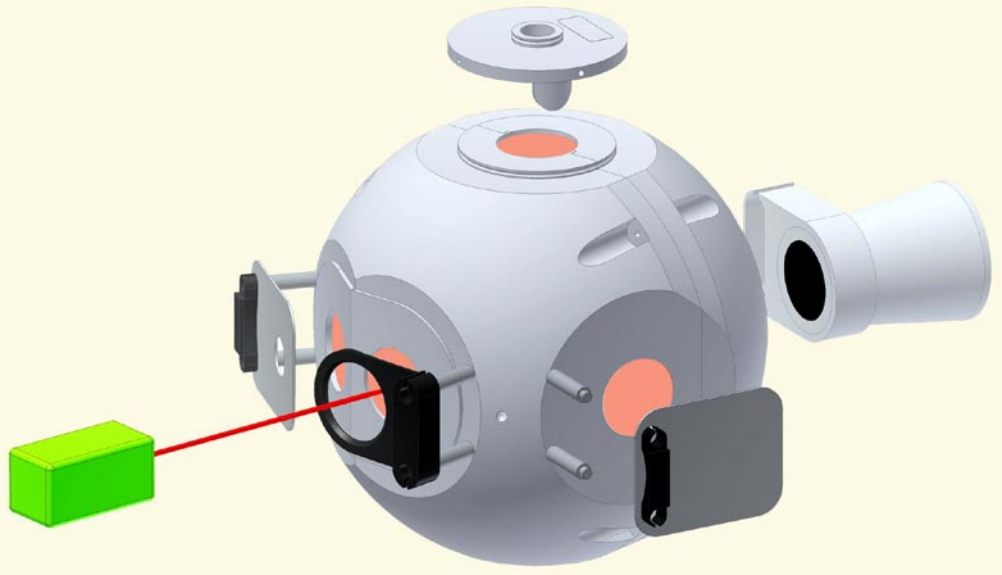

Figure 2.1: Integrating sphere for reflectance and transmittance measurement. *Figure taken from: www.thomasnet.com*

2.2.1 Direct methods

These methods are using very simple principles of light propagation such as Lambert-Beer law, single scattering phase function, etc [5]. This is advantageous for simple physical interpretation and no need of more complicated theoretical model. Optical properties are then calculated directly from measurement of absorbed or scattered fraction of light [65]. On the other hand they are limited by the requirements on the sample preparation and hence they are not suitable for in vivo measurements. For example satisfying single scattering sample for phase function measurement can be very problematic. And although this methods are simple in principle, it can be difficult to provide measurements [21]. Direct method was used for example by Treweek *et al.* [58], using 20-120 μm thick samples of human breast skin.

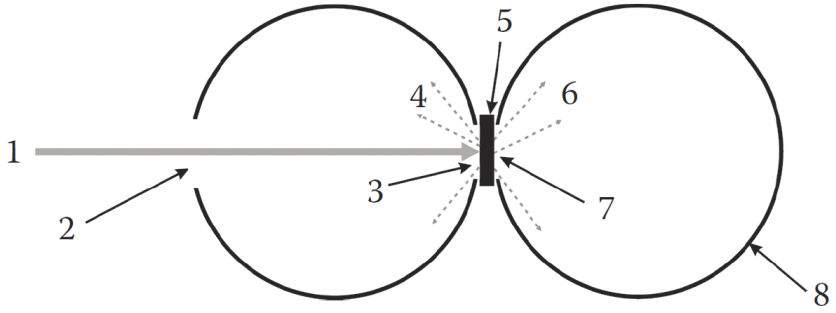

Figure 2.2: Double integrating sphere for simultaneous transmittance and reflectance measurement: (1) incident beam, (2,7) entrance port, (3) exit port, (4) diffuse reflected photons, (5) sample, (6) transmitted photons, (8) integrating sphere. *Figure taken from: [5]*

2.2.1.1 Direct methods for thin samples

Mostly used measurement method is integrating sphere as was mentioned before. Here is the description of measurement the most important coefficients [64]:

- Attenuation coefficient
  - for measuring total attenuation coefficient very simple measurement of collimated transmittance T_c through thin sample can be used , see Fig. 2.3(a)
  - it can be described by following equation:

$$\mu_t = -\frac{1}{d} \ln T_c, \tag{2.1}$$

    where d is sample thickness

- Absorption coefficient
  - for determination of the absorption coefficient total transmittance is measured and hence only absorption is responsible for the loss in the sample:

$$\mu_a = -\frac{1}{d} \ln \left(\frac{N_a}{\eta N_0} \right), \tag{2.2}$$

    where d is sample thickness, η fraction of all photons detected by highly diffuse reflective coating , N_0 number of incidence photons and N_a is number of detected photons, see Fig. 2.3(b)

- Scattering coefficient
  - analogically we can measure scattering coefficient, see Fig. 2.3(c):

$$\mu_s = -\frac{1}{d} \ln \left(1 - \frac{N_s}{\eta N_0} \right). \tag{2.3}$$

- Scattering phase function
  - phase function can by measured by rotating collimated detector around the sample, see Fig. 2.3(d)

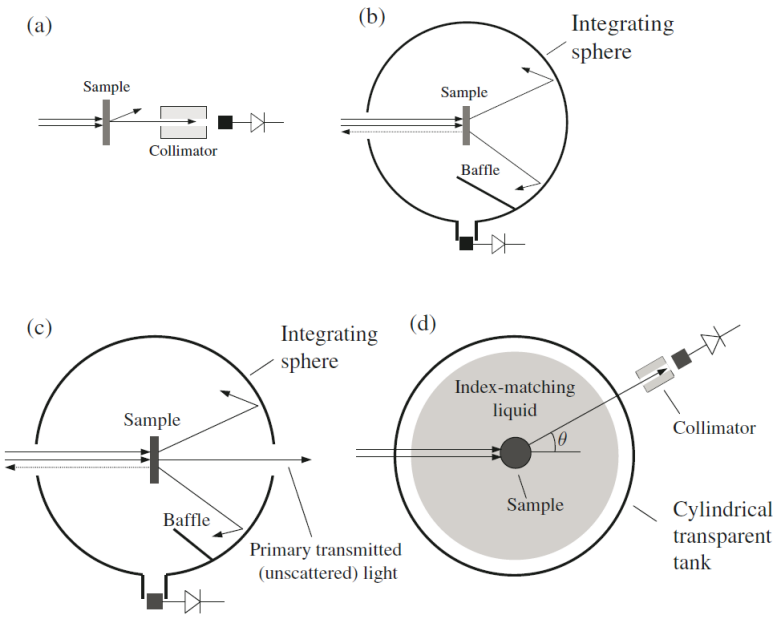

Figure 2.3: Direct methods in thin samples. Measurement of: (a) total attenuation coefficient μ_t, (b) absorption coefficient μ_a, (c) scattering coefficient μ_s, (d) scattering phase function (θ). *Figure taken from: [64]*

Satisfying right conditions for measurement is often problematic. For instance multiple scattering has to be negligible and for the range of tissue optical properties it means sample less than $10\mu m$ thin. It is also hard to satisfy optically smooth surface and detected signal is usually very low [64].

2.2.2 Indirect methods

Several different theoretical models or numerical methods can be used, the most common are: two-flux and multi-flux models, the IMC or IAD methods [5].

2.2.2.1 Inverse Adding doubling

This method was described in general in Section 1.3.4 as method of modeling light transport within the tissue. In the inverse adding-doubling method total reflection, total transmission and collimated transmission measurements are used for calculation scattering, absorption and scattering anisotropy values. The advantage over existing methods are accuracy and flexibility in modeling turbid samples with intermediate albedos, mismatched boundary conditions and anisotropic scattering. It is used for optical property determination of the tissue ex vivo, typically with double and single-integrating spheres for reflectance and transmission measurement [2, 45]. Process of algorithm implementation is shown in Figure 2.4.

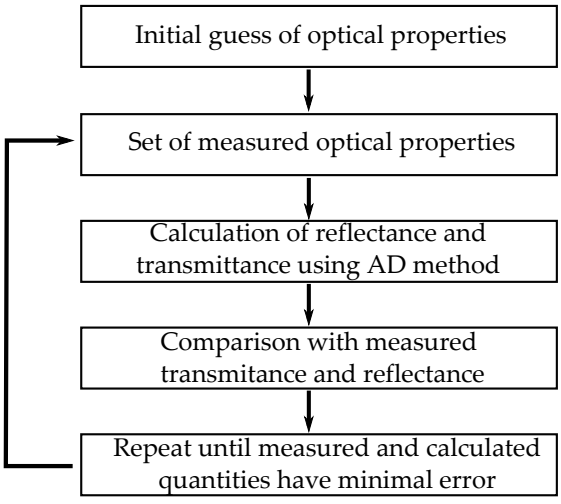

Figure 2.4: Flowchart of inverse Adding-doubling method.

2.2.2.2 Multiple polynomial regression

In addition to the commonly used methods, Dam *at al.* [14] introduced a new method. It is based on combining Monte Carlo simulation, multiple polynomial regression and a Newton-Raphson algorithm for solving nonlinear equation system. First, the Monte Carlo simulation is used for mappings of relevant subsets of μ_a, μ_s' space onto their images in reflectance and transmittance spaces. For further processing mathematical description of T and R is needed. It was found out that these images requires relatively simply mathematical functions for description and hence they are fitted with double polynomials. Final step is using Newton-Rapson algorithm for solving inverse problem.

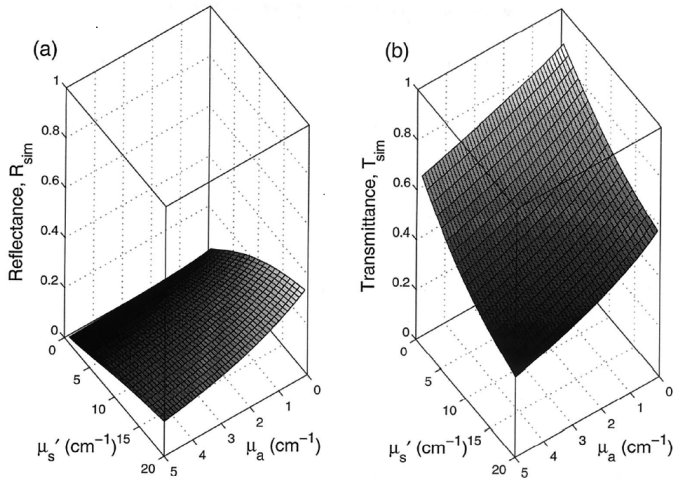

Figure 2.5: Reflectance and transmittance images. *Figure taken from [14]*

This method was also used in spatially resolved measurement of diffuse reflectance as will be discussed later.

2.3 In-vivo methods

Importance of these methods lies in non-invasive use and therefore they are more useful for practical applications in medicine than ex vivo. On the other hand, due to the requirements on sample thickness direct methods are no longer possible and indirect methods are employed. Indirect methods measure macroscopic parameters (transmittance, reflectance), from which the tissue optical properties are obtained by solving inverse problem. Inverse problem is based on one of the models of light propagation described in Chapter 1. Approximations for simplification are often used for the modeling - mostly the tissue is assumed to be semi-infinite medium with uniformly distributed scattering and absorption center. Indirect methods are limited in accuracy by ability of the model to describe the specific experimental conditions. Hence

finding the accurate and simple model is the main target. We can divide methods from several aspects into subcategories [64]:

- **Measurement geometry**
  - Reflectance measurement
  - Transmittance measurement
- **Measured quantity**
  - Intensity
  - Fluence rate
  - Radiance
- **Illumination source**
  - Steady state: for determination of tissue optical properties we can use following approaches:
    - *Spatially resolved*
    - *Spectrally constrained*
  - Time dependent: they are suited for deeper examination ($> 1\ cm$) in the tissue. For determination of tissue optical properties we can use following approaches:
    - *Time resolved* - it uses picosecond pulses and measure the impulse response of the tissue
    - *Frequency domain* - it relies on determination of the phase shift and amplitude modulation, incident beam is frequency modulated [64]

Further we can divide methods on iterative and non-iterative. Diffuse reflectance measurement is nowadays mostly used method of measurement. It can be used with several different models as diffusion theory, Monte Carlo, Kubelka-Munk or relatively new empirical models.

2.3.1 Diffuse reflectance measurement

Total diffuse reflectance is defined as: "the fraction of light re-emitted through the front (irradiated) surface" [64]. Two methods for total diffuse reflectance measurement are shown in Figure 2.6. Integrating sphere is not commonly used for its high price. On the other hand because of accurate results it has its applications. Methods using CCD and laser source are very popular and are commonly used nowadays. Next possible method is fiber optic probe shown in Figure 2.8.

Basically it is not possible to determine coefficients μ_s' and μ_a only from total diffuse reflectance R_d measurement. We need to use certain distinction

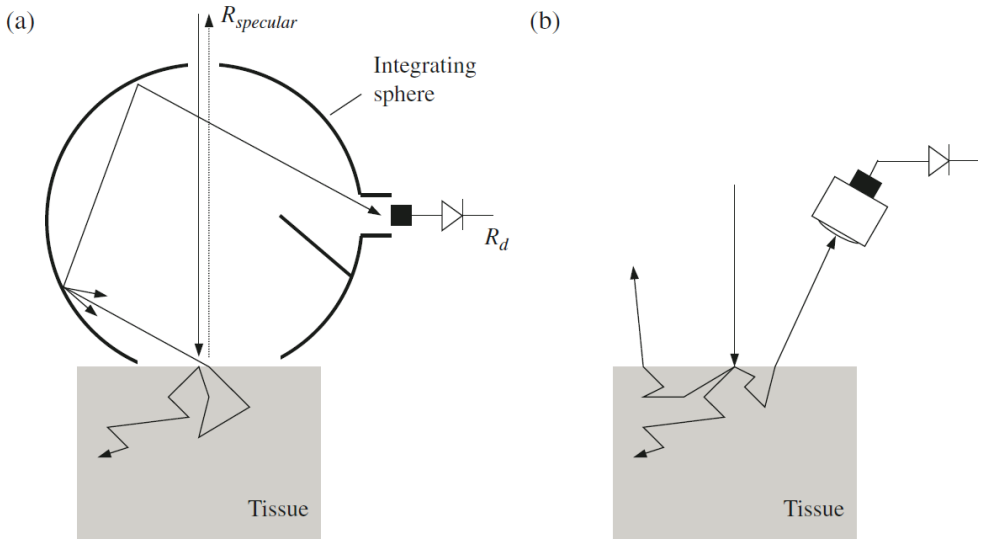

Figure 2.6: Total diffuse reflectance measurement with (a) integrating sphere, (b) distant detector. *Figure taken from: [64]*

as spatially resolved or spectrally constrained measurement. Total diffuse reflectance R_d can be expressed as function of μ_s', μ_a and g (and if including surface refractive index mismatch also n). A formula for diffuse reflectance can be derived from diffusion theory [21]:

$$R_d = \frac{a'}{1 + 2\kappa(1 - a') + (1 + \frac{2\kappa}{3})\sqrt{3(1 - a')}}, \tag{2.4}$$

where a' is reduced albedo, $\kappa = \frac{1+r_{id}}{1-r_{id}}$ and r_{id} is the internal reflection coefficient for diffuse light. Value of r_{id} depends whether index of refraction matches at the surface.

$$r_{id} = \begin{cases} 0 & for\ matching \\ 0.46 - 0.60 & for\ mismatching\ (for\ n_{tissue} = 1.3 - 1.5) \end{cases}$$

Models for solving inverse problems are often based on diffusion approximation to the radiative transfer theory, which was described in Section 1.3.1. But as was mentioned before, diffusion theory has its limitations and therefore exists many other models to overcome these limitations. As it was previously written we can measure diffuse reflectance in different ways, results from different types of measurements are shown in Figure 2.7 (details will be described in corresponding subsections). We will describe principles of measurement in each category and we will introduce algorithms and models for determination tissue optical properties.

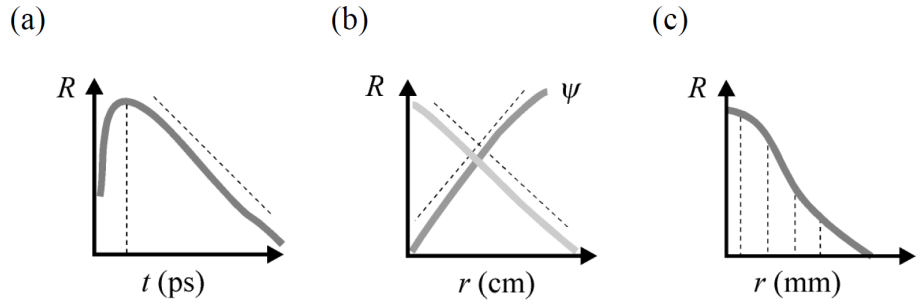

Figure 2.7: Reflectance spectra from: (a) time resolved measurement, (b) frequency domain measurement, (c) spatially resolved measurement. *Figure taken from: [12]*

2.3.1.1 Spatially resolved steady state diffuse reflectance

In this methods the reflectance is measured as a function of the distance from the source $R_d(r)$. In Figure 2.8 we can see two dominant ways of measurement - fiber probe and CCD with laser as a source.

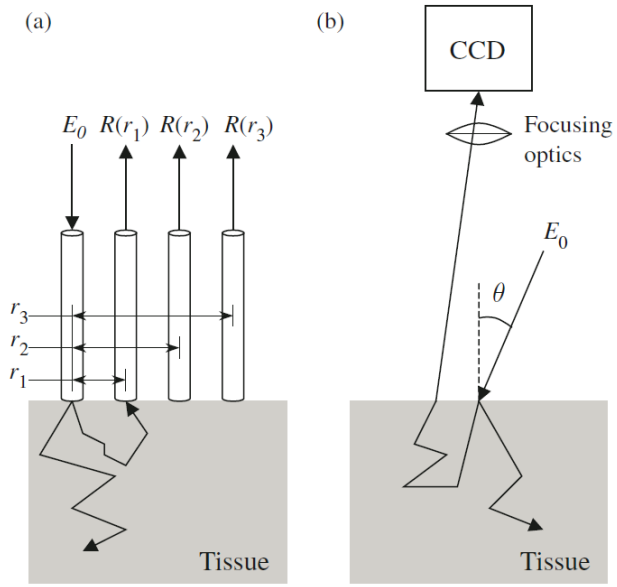

Figure 2.8: Methods for measurement spatially-resolved diffuse reflectance. (a) Fiber probe, (b) CCD with laser or collimated beam irradiation. *Figure taken from: [64]*

Commonly used determination methods use fitting the shape of $R_d(r)$ curve to the analytical equation. The analytical solution is often based on the diffusion

theory and probably the most important and cited model was introduced by Farrell *at al.* [18]. Number of later papers are based on this model, for example from Kienle *at al.* [30]. Final result of analytical expression for diffuse reflectance is:

$$R(r) = \frac{a'}{4\pi}\left[\frac{1}{\mu_t'}\left(\mu_{eff}+\frac{1}{r_1}\right)\frac{e^{(-\mu_{eff}r_1)}}{r_1^2}+\left(\frac{1}{\mu_t'}+2z_b\right)\left(\mu_{eff}+\frac{1}{r_2}\right)\frac{e^{(-\mu_{eff}r_1)}}{r_2^2}\right] \tag{2.5}$$

$$r_1 = \left[\left(\frac{1}{\mu_t'}\right)^2+r^2\right]^{1/2} \tag{2.6}$$

$$r_2 = \left[\left(\frac{1}{\mu_t'}+2z_b\right)^2+r^2\right]^{1/2}, \tag{2.7}$$

where μ_{eff} is effective attenuation coefficient, μ_t' is reduced attenuation coefficient and z_b is the distance from surface to the extrapolated boundaries. Handling boundary conditions is very important for model based on diffusion theory.

Due to the limitations of diffusion theory different models were developed (mainly for fiber probe measurement with typically small distances between source and detector fiber). One of the methods introduced by Dam *at al.* [15] is based on the multiple polynomial regression - MPR. In this algorithm $R_d(r)$ is firstly measured at two distances r_1 and r_2 for a set of calibration sample – $R_{1,cal}$ and $R_{2,cal}$. Then the double polynomial fit is used and inverse problem is solved on a set of prediction samples. In the end a Newton-Ralphson algorithm is used to perform converging iterative calculations.

Next group of methods is using neural network for determining the optical properties. This methods does not rely on diffusion approximation and thus are applicable for any combination of scattering and absorption coefficient. First method from Kienle *et al.* [30] uses laser source and CCD sensor as

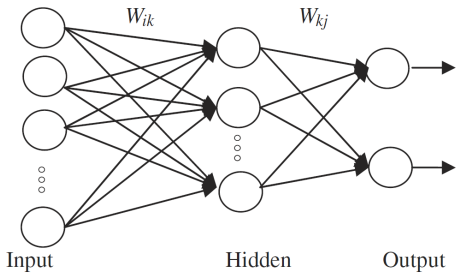

Figure 2.9: Structure of neural network. *Figure taken from: [69]*

detector and for determination of the optical properties NN trained on the results of Monte Carlo simulation is used. Two networks are employed for calculation - first has 11 input nodes, 11 hidden nodes and 2 output nodes, second has 9 input nodes, 9 hidden nodes and 2 output nodes. Output nodes are represented by μ_t' and μ_{eff} and from these parameters the scattering and the absorbing coefficients are calculated. Training NN requires long times, but after that the calculation is very fast. Example of another method is in the paper from Yagin *et al.* [67]. As improvement they uses principal component analysis (PCA) for preprocessing to compress the data set.

2.3.1.2 Spectrally constrained measurement

Spectrally constrained measurement of diffuse reflectance $R_d(\lambda)$ is second type of steady state measurement. Principle of measurement is shown in Figure 2.10. Major application of these methods is study of specific chromophores in

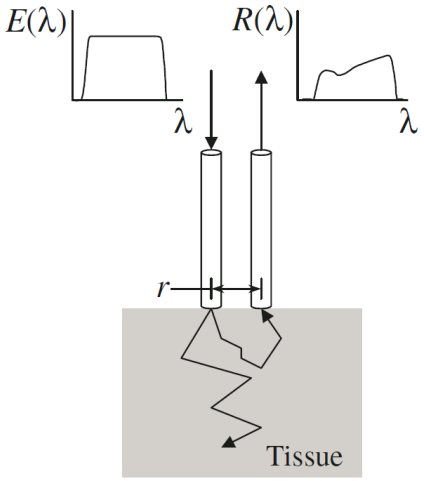

Figure 2.10: Principle of spectrally constrained diffuse reflectance measurement. *Figure taken from: [64]*

the tissue [64]. The main chromophores in the tissue are water, oxyhemoglobin and deoxyhemoglobin. These are the most important and they contributes significantly to the total absorption - others can be melanin, lipids, etc. The apriori knowledge of the absorption and scattering spectra is needed for extracting of optical properties. Therapeutic window is mostly used wavelength region In this range scattering is dominant over absorption and therefore fulfill the requirement for diffusion theory. There are several models for spectra calculation and they are dependent on the type of the tissue and on the range of wavelength (in some regions we can neglect some chromophore for their low absorption). We will describe the modeling of absorption and scattering spectra:

Absorption spectrum is usually modeled by linear combination of the main contributors. Absorption spectra of water were already well described by Matcher *et al.* [38]. Spectra for other main chromophores can be found in work from Branco [6]. We were briefly discussing this topic in Chapter 1. Absorption coefficient can be calculated as:

$$\mu_a(\lambda) = \sum_i c_i \cdot \epsilon_i(\lambda) \ , \tag{2.8}$$

where c_i is the chromophore concentration and ϵ is molar extinction coefficient. The main chromophores in the NIR region are water and hemoglobin and hence others chromophore are often negligible. For known absorption coefficient of each chromophore we can use model in Equation 2.9 [64]. Final spectrum is calculated as combination of water content, hemoglobin concentration and oxygen saturation:

$$\mu_a(\lambda) = c_{water}\mu_a^{water}(\lambda) + c_{Hb}^* \left[StO_2\mu_a^{HbO_2}(\lambda) + (1 - St0_2)\,\mu_a^{Hb}(\lambda) \right] \tag{2.9}$$

- $\mu_a^{water}(\lambda)$ - spectra for water
- $\mu_a^{HbO_2}(\lambda)$ - spectra for oxynated hemoglobin
- $\mu_a^{Hb}(\lambda)$ - spectra for deoxynated hemoglobin
- c_{water} - volume fraction of water
- c_{Hb}^* - volume fraction of total hemoglobin
- $St0_2$ - oxygenation fraction

Similar model is often used in various papers [71, 73].

Scattering - real tissue description of single scatterers is very complicated for modeling . But research has shown it can be easily described by power law [64]:

$$\mu_s'(\lambda) = a\lambda^{-b} \tag{2.10}$$

- a - scattering magnitude
- b - scattering power

Diffusion approximation is very often used type of approximation and hence lot of spectrally constrained measurement are using this model as well. One classical model based on diffusion approximation was described by Zonios *et al.* [73]. It is based on the model from Farrel *et al.* [18] (Equation 2.5, only with fixed value of r). Measured tissue were human adenomatous colon polyps and spectra was calculated as:

$$\mu_a(\lambda) = \log_e 10 c_{Hb}^* [\alpha\epsilon_{Hb0_2}(\lambda) + (1 - \alpha)\epsilon_{Hb}(\lambda)] \tag{2.11}$$

$$\alpha = (c_{HbO_2})/(c_{HbO_2} + c_{Hb}) \tag{2.12}$$

$$c_{Hb}^* = c_{HbO_2} + c_{Hb}, \tag{2.13}$$

where α is hemoglobin oxygen saturation parameter (or oxygenation fraction) and $c_{Hb}*$ is hemoglobin total concentration. Because it is very difficult to describe every single scatterer here was used an average model. It was modeled as if tissue contains only one type of scatterers.

$$\mu_s' = \rho_s \sigma'(\lambda) \tag{2.14}$$

where ρ_s is effective scattering density and $\sigma'(\lambda)$ the effective reduced scattering cross section.

Diffusion theory fails for small detector separation from the source. It can be problematic for endoscopic use, while the dimension of the optical part of probe head is about 3 mm [51]. Therefore empirical models were introduced for possibility of using fiber probes [1, 51, 71]. One interesting model was proposed by Reif *et al.*[51]. We will describe the model development because this is the area we are interested in. The probe with source detector separation 250 nm is used for the measurement and diffuse reflectance was measured with fibers tilted under different angles (Figure 2.11). First, diffuse reflectance as

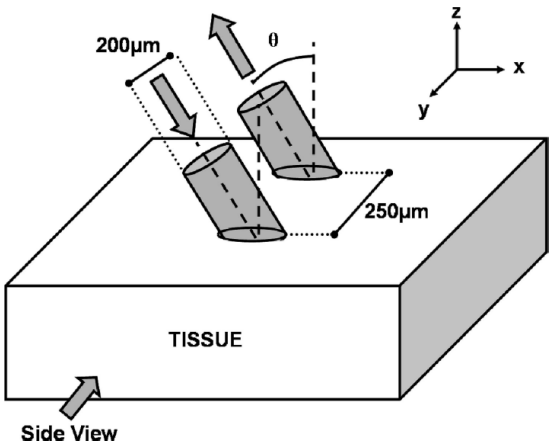

Figure 2.11: Diffuse reflectance measurement with tilted fiber. *Figure taken from [51]*

a function of the reduced scattering coefficient was expressed:

$$R_d(0) = a_1 \mu_s' + a_0. \tag{2.15}$$

This is a simple equation describing diffuse reflectance in medium with zero absorption. Parameters a_0 and a_1 were determined both for Monte Carlo simulation and for real measurement on the tissue phantoms with well known optical properties. Model was further developed by adding the dependence on

the absorption coefficient:

$$R_d = R_d(0)(-\mu_a < L >) \tag{2.16}$$

$$L = \frac{b}{(\mu_a \mu_s')^c}, \tag{2.17}$$

where parameters b and c were determined in the same manner as a_1 and a_0. In the later paper from Calabro *et al.* [7] this model was further developed:

$$R_d = (a_4 \mu_s'^4 + a_3 \mu_s'^3 + a_2 \mu_s'^2 + a_1 \mu_s' + a_0) \exp(-\mu_a \frac{b}{(\mu_a \mu_s')^c}). \tag{2.18}$$

This model provides better description compared to the original model by using higher order polynomial terms for describing diffuse reflectance in non-absorbing medium.

Another empirical model was introduced by Zonios *at al.* [71]. It is based on simple exponential model and the deducing of the model will be described in Chapter 3. Model was validated on tissue simulating phantoms and later it was used on skin tissue. One of the major chromophore in the skin is melanin and spectra were modeled as:

$$\mu_a(\lambda) = c^*_{Hb} \left(\alpha \epsilon_{Hb0_2}(\lambda) + (1-\alpha)\epsilon_{Hb}(\lambda)\right) + c_{mel}\epsilon_{mel}(\lambda) \tag{2.19}$$

$$\mu_s'(\lambda) = \left(1 - \sqrt{\frac{d_0}{d_s}}\right) \mu_s'(\lambda_{min}), \tag{2.20}$$

where d_s is effective scatterer size, $d_0 = 0.0625 \mu m$ constant, $\lambda_{min} = 450nm$, $\lambda_{max} = 900nm$ and others were described before. Empirical models are relatively new compare to diffusion approximation but it has been proved that they are capable of determining optical properties with the similar accuracy.

2.3.1.3 Time resolved measurement

Time resolved reflectance methods are based on measurement of the impulse response of the tissue. The input signal is picosecond pulse and the reflectance is measured as a function of time in a distance near by source. These methods are advantageous due to possibility of optical properties determination from direct metrics as final logarithmic slope and time-to-maximum. Principle of measurement is shown in Figure 2.12. Index of refraction is needed for calculation of speed of light moving within the tissue. Commonly used value is $1.35 - 1.45$, we will assume $n = 1.4$:

$$c_t = \frac{c}{n} = 214137470 \; m \cdot s^{-1} = 0.21 \; mm \cdot ps^{-1}. \tag{2.21}$$

With knowledge of average path length l we can calculate average time delay:

$$t = \frac{l}{c_t}. \tag{2.22}$$

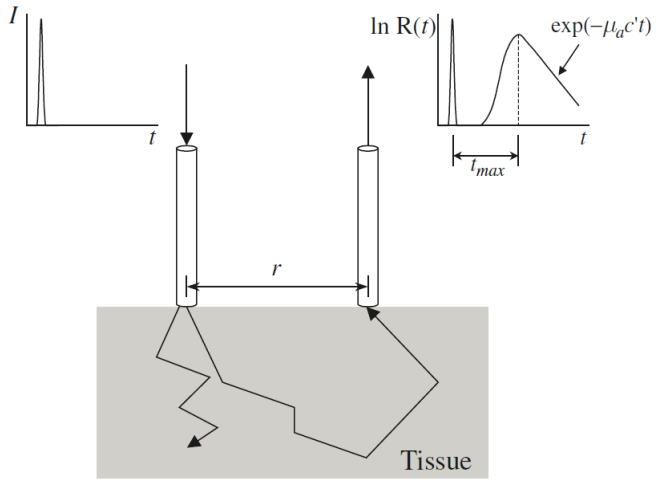

Figure 2.12: Time-resolved diffuse reflectance measurement. *Figure taken from: [64]*

This is the definition of the basic units used in these methods [64].

Diffusion theory adjusted for the time resolved measurement is again commonly used [44]. Diffuse reflectance is then given by:

$$R(r,t) = (4\phi D c_t)^{-3/2} z_0 t^{-5/2} \exp(-\mu_a c_t t) \exp\left(-\frac{r^2 + z_0^2}{4 D c_t t}\right), \tag{2.23}$$

where $z_0 = 1/[\mu_s(1-g)]$. In the case $r^2 >> z_0^2$ by using simple adjustment we obtain:

$$\frac{\partial}{\partial t} \log_e R(r,t) = -\frac{5}{2t} - \mu_a c_t t + \frac{r^2 + z_0^2}{4 D c_t t} \tag{2.24}$$

$$\lim_{t\to\infty} \frac{\partial}{\partial t} \log_e R(r,t) = -\mu_a c_t. \tag{2.25}$$

Absorption coefficient can be determined from the logarithmic slope of the time-dependent diffuse reflectance curve. Reduced scattering coefficient can be determined by suggesting that slope of curve is zero at t_{max} (time with maximum measured signal):

$$\mu_s' = \frac{1}{3r^2}(4\mu_a c_t^2 t_{max}^2 + 10 c_t t_{max}) - \mu_a. \tag{2.26}$$

This method was validated on the tissue simulating phantoms with error under 10%. Another method using diffusion approximation was introduced by Svensson *et al.*[56]. It was designed for interstitial measurement of prostate tissue for cancer detection. Experimental data was fitted with equation:

$$y(\mu_a, \mu_s', k, t) = k t^{-3/2} \exp\left(-\frac{3\mu_s' r^2}{4 c_t t} - \mu_a c_t t\right), \tag{2.27}$$

where k is free parameter carrying amplitude information. Best fit was ensured by Lavenberg-Marquard algorithm. Data was measured at three wavelength 660, 786 and 916nm at three distances 15, 20 and 25mm. In their previous research they were investigating breast tissue for diagnosis of breast cancer. Use of multiple wavelengths enable determination of main tissue chromophores [55]. Instrumentation is shown in Figure 2.13.

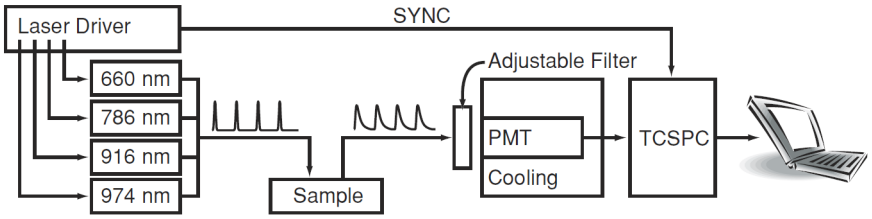

Figure 2.13: Instrumentation for time resolved measurement: TCSPC - time correlated single photon counting, PMT - photonmultiplier tube. *Figure taken from [55]*

Interesting Monte Carlo method was developed by Kienle *et al.* [31]. Because numerical methods are often limited in their speed of calculation, in this method a single Monte Carlo simulation is used. This is possible only for known value of anisotropy factor and refractive index (it can be assumed for biological tissue). Basic principle is extraction of reflectance data from the output of simulation with well known scattering coefficient and absorption coefficient. We will use an simple example to explain: Monte Carlo simulation is performed with parameters μ_{ar}, μ_{sr} and reflectance obtained from simulation is donate R_{dr}. For $\mu_{ar} = 0$ we can use simple equation for calculation of diffuse reflectance for any value of μ_a:

$$R_d(r,t) = R_{dr}(r,t)e^{-\mu_a c_t t}. \tag{2.28}$$

For this case we can calculate diffuse reflectance for arbitrary value of scattering coefficient:

$$R_d(r,t) = \left(\frac{\mu_s}{\mu_{sr}}\right)^3 R_{dr}(r\frac{\mu_s}{\mu_{sr}}, t\frac{\mu_s}{\mu_{sr}}). \tag{2.29}$$

Diffuse reflectance can be then easily calculated for any values of absorption and scattering coefficient by using Equations 2.28 and 2.29. This method is accurate also for very large value of absorption coefficient and measurement close to the source ($r = 2.5/\mu_s'$). This method can be applied also with the frequency domain measurement by Fourier transformation [31].

We will shortly describe more methods using time resolved reflectance. Chernomordik *et al.* [10] introduced method based on random walk theory. It

is mathematical method for describing stochastic process like light distribution in the tissue. It was well described by Ren *et al.* [52]. Their concept was to separate absorption from scattering for better tissue analysis. It is possible because early time response of the tissue is mainly corresponding to scattering while later to absorption. Time resolved measurement in multi layered media was introduced as well. Solution of diffusion equation for multi layered media was presented by Martelli *et al.* [37]. This issue was also well described and used in methods from Kienle *et al.* [29]. They use Monte Carlo simulation for skin, subcutaneous fat and muscle modeling. In their previous research [32] they introduced experimentally determined relation for diffuse reflectance (with assumption of all photons scattered isotropically at depth $z = z_0 = 1/(\mu_a + \mu_s')$ and refractive index above the medium $n = 1$ and $n_{tissue} = 1.4$):

$$R(r,t) = 1.118\Phi(r, z = 0, t) + 0.306D\frac{\partial}{\partial z}\Phi(r, z, t)|_{z=0}. \tag{2.30}$$

Fitting at two distances enable determination of first layer thickness and both absorption and reduced scattering coefficient for first two layers.

2.3.1.4 Frequency domain measurement

In frequency domain reflectance measurement the light source intensity is modulated at different frequencies. It is analogical to the Fourier transform of time resolved measurement and carries no additional information. But still has its advantages in acquisition time and data analysis. On the other hand the problem is relative large source detector separation (in cm) [12]. Measured variables are phase Ψ and amplitude modulation M[5] of diffuse reflectance. Both measurement at low and high frequencies can be used, although high frequencies modulation prevails. At low frequencies $2\pi f << \mu_a c_t$ applies $M = 1$ and:

$$\Psi = \frac{\pi(\mu_{eff} r_0)^2 f}{\mu_a c_t (1 + \mu_{eff} r_0)}, \tag{2.31}$$

where $r_0 = r^2 + z_0^2$ and $z_0 = 1/\mu_s'$. But only measurement in frequency domain is not sufficient for determination both μ_s' and μ_a and some additional measurement has to be performed. That is because of proportional value of phase Ψ to frequency. But in this range of frequencies ($f < 200Hz$)), low cost equipment is the main advantage [64].

Combining spectrally constrained and frequency domain measurements is an often used solution for determination optical properties simultaneously with physiological parameters. These methods were introduced by many researchers: for example Pantini *et al.* [17] and Fishkin *et al.* [19]. In the second paper light source was high-bandwidth with frequency modulation in

[5] amplitude modulation is defined as ratio between average intensity and the amplitude of the intensity oscillations [59]

range $0.3MHz - 1GHz$. For phase shift determination was used expression introduced by Haskel *et al.* [23]:

$$\Psi(\mu_a, \mu_s', r, \omega) = k_{imag} r_0 - \arctan \frac{IMAG}{REAL}, \tag{2.32}$$

where:

$$\begin{aligned}
REAL &= \frac{\exp(-k_{real})r_0}{r_0} - cos[k_{imag}(r_{ob} - r_0)] \times \frac{\exp(-k_{real} r_{ob})}{r_{ob}} \\
IMAG &= \sin[k_{imag}(r_{ob} - r_0)] \frac{\exp(-k_{real} r_{ob})}{r_{ob}} \\
k_{real} &= \left(\frac{3}{2}\mu_a \mu_s'\right)^{1/2} \left\{ \left[1 + \left(\frac{\omega}{c_t \mu_a} \right)^2 \right]^{1/2} + 1 \right\}^{1/2} \\
k_{imag} &= \left(\frac{3}{2}\mu_a \mu_s'\right)^{1/2} \left\{ \left[1 + \left(\frac{\omega}{c_t \mu_a} \right)^2 \right]^{1/2} - 1 \right\}^{1/2} \\
r_0 &= \left[\left(\frac{1}{\mu_s'} \right)^2 + r^2 \right]^{1/2} \\
r_{ob} &= \left[\left(2z_b + \frac{1}{\mu_s'} \right)^2 + r^2 \right]^{1/2} \\
z_b &= \frac{1 + R_{eff}}{1 - Reff} \cdot \frac{2}{3\mu_s'},
\end{aligned} \tag{2.33}$$

where R_{eff} is effective reflection coefficient and ω is angular intensity-modulation frequency of the source. Because measurement at multiple wavelengths was employed, an additional quantities as hemoglobin concentration and blood saturation can be measured. In paper from Bevilacqua *et al.* [3] was used frequency domain measurement in combination with spectrally constrained as well. Procedure is as follow:

1. values of μ_s', μ_a was determined from frequency domain measurement
2. these values were used for calibration of intensity of steady state measurement
3. estimation of μ_s'
4. estimation of μ_a by comparing steady state reflectance values with the prediction of diffusion theory.

It is advantageous to measure over a range of frequencies for more accurate results. In this case frequency of the source (network analyzer) varies from 100 to 700 MHz.

To summarize this category it often uses additional measurement for obtaining for example physiological information. These methods are rather complicated and requires relatively expensive equipment.

CHAPTER 3

Method design

In previous chapter we have summarized methods used for tissue optical properties determination. Now we can discuss which method fulfills our requirements and therefore it is the most suitable for our application. Firstly we can exclude methods using integrating sphere because of ex vivo measurement and expensive equipment. Reasonable choice is hence diffuse reflectance measurement, as it can be accurate and we can choose from several models. Due to expensive equipment, we need to exclude time resolved and frequency domain measurement as well. But recent studies have shown that method based on spatially resolved and spectrally constrained measurement achieve similar accuracy to time resolved and frequency domain methods. In spectrally constrained measurement the knowledge of absorption and scattering spectra is needed. This can be limited for measurement in tissue with unknown or inaccurately described spectra. Therefore for its universality we are focusing on spatially resolved measurement. Our fiber probe used for phantom measurement has very small source-detector separation - less than 1 mm and hence we can exclude diffusion approximation with the requirements on source detector separation:

$$SDS >> mfp. \tag{3.1}$$

We reject also inverse Monte Carlo method because of calculation complexity. Therefore after considering all circumstances we get to the empirical model. It is relatively new approach, compared to the diffusion approximation and inverse Monte Carlo method [7]. In previous chapter we have described several methods using this empirical models and their results are comparable to other methods.

3.1 Model development

The main aim of this project is to develop new method based on spatially resolved diffuse reflectance measurement. We are focusing on measurement in small volumes and therefore we are using very small source detector separation (less than $1mm$). The main requirement remains model simplicity but with good physical approximation. Very reasonable model was developed by Zonios *et al.* [71]. But in this method spectrally constrained measurement is used and therefore some adjustment is needed. This model is based on very simple exponential model. In their later papers [72] they developed more empirical models in using data from Monte Carlo simulation and they are helpful in our model development. In summarization, our aim is to test whether spatially resolved measurement can be used for determination of the tissue optical properties even in very small distances from the source . It can be advantageous for example in endoscopic application, which requires primarily fast determination with simple equipment.

3.1.1 Exponential model

While simplicity is one of the main requirements we need to choose physical approximation with very simple basis. We follow the process introduced by Zonios *et al.* [71] based on exponential model. The tissue is assumed to be homogeneous semi-infinite turbid medium, which is a commonly used assumption. Light in the tissue is exponentially attenuated according to the reduced attenuation coefficient $\mu_t' = \mu_s' + \mu_s$. The incident light can be expressed as:

$$I = I_0 e^{-(\mu_s' + \mu_a)z}, \tag{3.2}$$

where I_0 is the light intensity on the surface ($z = 0$). For the backscattered light it is proportional to the reduced scattering coefficient and is exponentially attenuated.

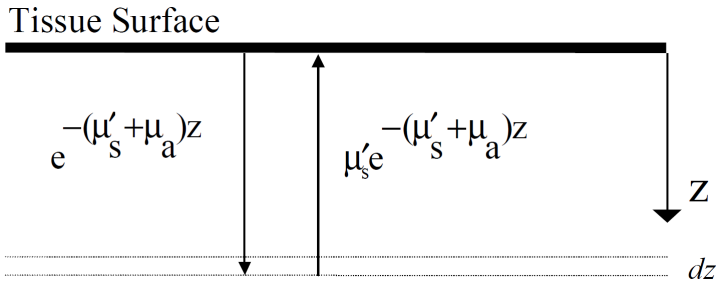

Figure 3.1: Basic model of exponentially attenuated light in the tissue. *Figure taken from: [71]*

Total diffuse reflectance can be written as:

$$R_d = 2\mu_s' \int_0^\infty e^{-2(\mu_s'+\mu_a)z} \mathrm{d}z = \frac{\mu_s'}{\mu_s' + \mu_a}. \tag{3.3}$$

With very simple examination we can test Equation 3.3 [6] whether it fulfills theoretical conditions. For very high value of absorption coefficient $\mu_a >> \mu_s'$ is $R_d \to 0$ as expected. For $\mu_a = 0$, diffuse reflectance equals one and it is proper behavior for semi-infinite medium. For better agreement with other models the reduced scattering coefficient was rescaled by an empirical factor k:

$$R_d = \frac{\frac{\mu_s'}{k}}{\frac{\mu_s'}{k} + \mu_a} = \frac{1}{1 + k\frac{\mu_a}{\mu_s'}} \tag{3.5}$$

In the range $\mu_s'/\mu_a = 1 - 1000$ is Equation 3.5 quite simple approximation. But in this form it is still not usable with real probe measurement because real probe measures only part of diffuse reflectance exiting from the surface.

3.1.2 First model

Our model is based on papers from Zonios *et al.* [70, 71]. They use semi-empirical model derived from simple exponential model 3.5. For use with fiber optic probe scale invariance has to be removed:

$$R_d = \frac{1}{k_1\frac{1}{\mu_s'} + k_2\frac{\mu_a}{\mu_s'}} \tag{3.6}$$

We can rewrite this equation as:

$$R_d = \frac{\mu_s'}{k_1 + k_2\mu_a} \tag{3.7}$$

This is very simple model and with use of diffuse reflectance spectroscopy is suitable for determining tissue optical properties. Coefficient spectra are modeled by Equation 2.19 described in previous chapter. But our requirements

[6] Solution of the integral:

$$\begin{aligned} R_d = 2\mu_s' \int_0^\infty e^{-2(\mu_s'+\mu_a)z} \mathrm{d}z = \left| \begin{array}{c} -2(\mu_s'+\mu_a) = t \\ -2(\mu_s'+\mu_a)\mathrm{d}z = \mathrm{d}t \\ \mathrm{d}z = \frac{\mathrm{d}t}{-2(\mu_s'+\mu_a)} \end{array} \right| = \\ = 2\mu_s' \int_0^\infty e^t \frac{\mathrm{d}t}{-2(\mu_s'+\mu_a)} = \frac{-\mu_s'}{\mu_s'+\mu_a}[e^t]_0^\infty = \frac{-\mu_s'}{\mu_s'+\mu_a}[e^{-2(\mu_s'+\mu_a)z}]_0^\infty = \\ = \frac{-\mu_s'}{\mu_s'+\mu_a}(0-1) = \frac{\mu_s'}{\mu_s'+\mu_a}. \end{aligned} \tag{3.4}$$

is spatially resolved measurement and therefore we need to express dependence of diffuse reflectance on the source-detector separation:

$$R_d(r) = \frac{\mu_s'}{k_1(r) + k_2(r)\mu_a}. \tag{3.8}$$

3.1.3 Second model

In further testing the original model showed relatively high errors. It is caused by inaccuracy in determination k_1 and k_2 coefficients. These coefficient exhibits its dependence also on reduced scattering coefficient. For this second model we use another model from the same research group [72]:

$$R_d(r) = \frac{k_1(r, \mu_s')}{1 + k_2(r, \mu_s')\frac{\mu_a}{\mu_s'}} \tag{3.9}$$

With data from Monte Carlo simulation we further develop this model.

3.2 Monte Carlo simulation

Code used for Monte Carlo simulation was developed by Quan Liu *et al.* [36], it is based on the work of Wang and Jacques [34]. Parameters of the simulation for the probe are shown in Figure 3.2.

Illumination Parameters

1	#Beam type:0-Collimated,1-Diffuse
0.01	#Beam radius(cm) The radius of center null area(cm)
0 1	#Beam radial and angular profile: 0-uniform, 1-Gaussian
0	#Incident angle (degree, w.r.t. the normal axis)
1.45	#Refractive index of illumination fiber
0.22	#Numerical Aperture of Illumination Fiber

Collection Parameters

1	#Employ collecting fibers
3	#The number of collecting fibers

#Fiber-Radius(cm)	Center-to-Center-Distance(cm)	Refractive-Index	Numerical-Aperture	Tilt-Angle
0.01	0.0250	1.47	0.22	0
0.01	0.0375	1.47	0.22	0
0.01	0.0500	1.47	0.22	0

Figure 3.2: Parameters used for Monte Carlo simulation: fiber probe.

3.2.1 Data processing and curve fitting

All data processing was performed in Matlab® Version 7.11.0.584. (R2010b) 64-bit version [57]. For fitting procedures Curve Fitting toolbox was used, which was very suitable and helpful for our model development.

3.2.2 Testing of basic model behavior

Before method implementation, we need to check whether model correspond with the theoretical assumptions. First, we need to confirm linear dependence of diffuse reflectance on reduced scattering coefficient for non-absorbing medium. After modification Equation 3.7 for non-absorbing medium we obtain:

$$R_d = \frac{\mu_s'}{k_1}. \tag{3.10}$$

This dependence was already tested by Johns *et al.* [28]. To confirm Equation 3.10 we perform Monte Carlo simulation and test this assumption for three different distances of detector from the source.

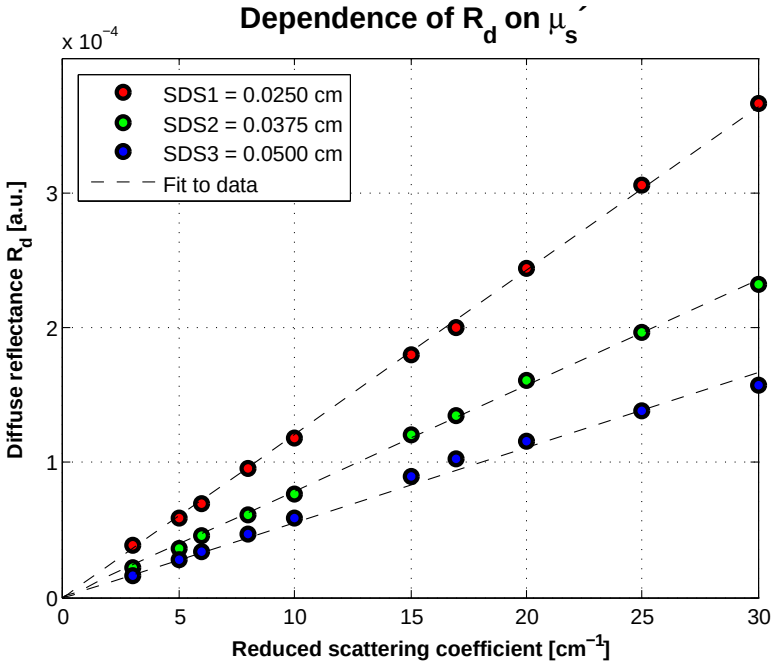

Figure 3.3: Dependence of diffuse reflectance on reduced scattering coefficient.

We can say that in non-absorbing medium the model describes simulated data accurately. Next step is to confirm decreasing dependence of diffuse reflectance on absorption coefficient. We perform Monte Carlo simulation and test ability of the model to fit data to Equation 3.7. Data was simulated for fiber 0.0250 *cm* distant from the source, results are in Figure 3.4. Simulation was performed for five different values of reduced scattering coefficient in the range of optical properties for the real tissue. Model fulfills our expectations and data are fitted accurately.

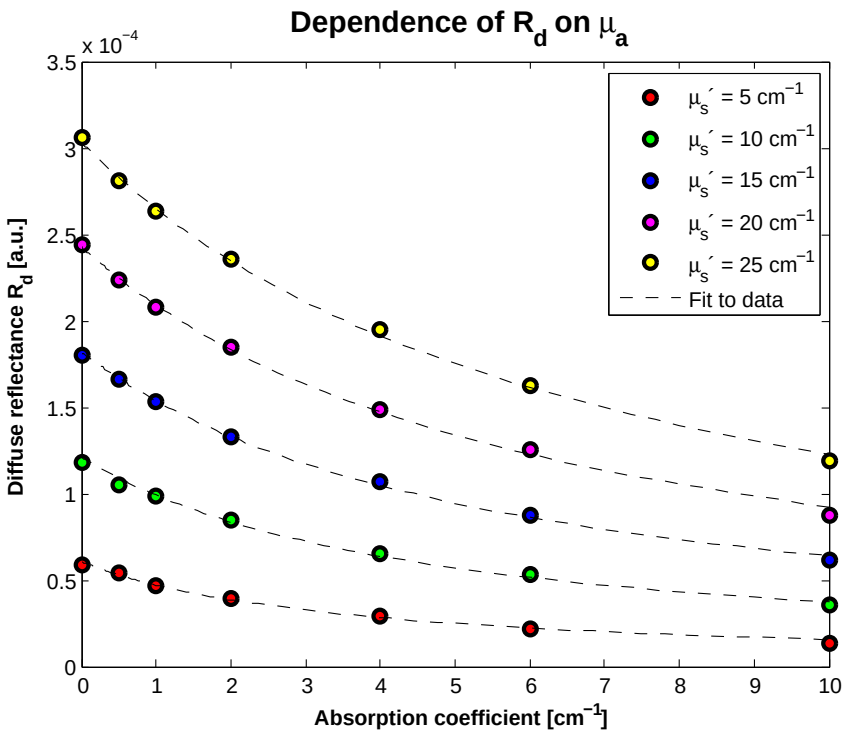

Figure 3.4: Dependence of diffuse reflectance on absorption coefficient, $SDS = 0.0250cm$.

3.2.3 Modification for spatially resolved measurement

Original models were used for spectrally constrained measurement and we need to modify them for spatially resolved measurement.

Model 1

For finding the dependence of parameters k_1 and k_2 on source detector separation we need to employ Monte Carlo simulation and fit data to Equation 3.7 with μ_a as independent variable. We obtain values of parameters k_1 and k_2 and we use Curve Fitting toolbox to express their dependence on source detector separation. Result from fitting is shown in Figure 3.7. We fitted both parameters with power law, but for final model we set the dependence for k_1 as linear dependence. It is because the power was close to one. Parameter k_2 is fitted with power law:

$$k_1 = a_1 r \tag{3.11}$$
$$k_2 = a_2 r^{b_2} \tag{3.12}$$

And by combining these equations with Equation 3.7 we get final model

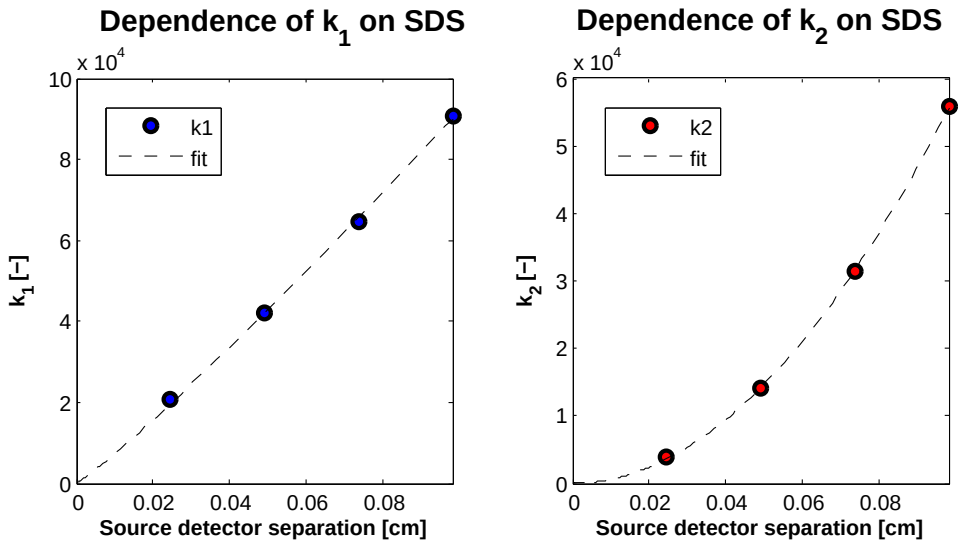

Figure 3.5: Dependence of parameters k_1 and k_2 on source detector separation.

for fitting procedure:

$$R_d(r) = \frac{\mu_s'}{a_1 r + a_2 r^{b_2} \mu_a}. \tag{3.13}$$

This is very simple empirical model and fits the data very well. We will continue with phantom study.

Model 2

We proceed in the similar manner as with the first model. The difference is only in three step calibration. First, we determine the dependence of coefficients k_1 and k_2 on reduced scattering coefficient and after that their dependence on source-detector separation. Dependence on reduced scattering coefficient is shown in Figure 3.6. Once we have determine the dependence, we can express it by using following expressions:

$$k_1(\mu_s') = a_1 \mu_s' \tag{3.14}$$
$$k_2(\mu_s') = a_2 \mu_s' + b_2. \tag{3.15}$$

Now we need to relate dependence of parameters k_1 and k_2 on source detector separation. We can do it through parameters a_1 and a_2, parameter b_2 is constant for all distances. Their dependence on source detector separation is shown in Figure 3.7.

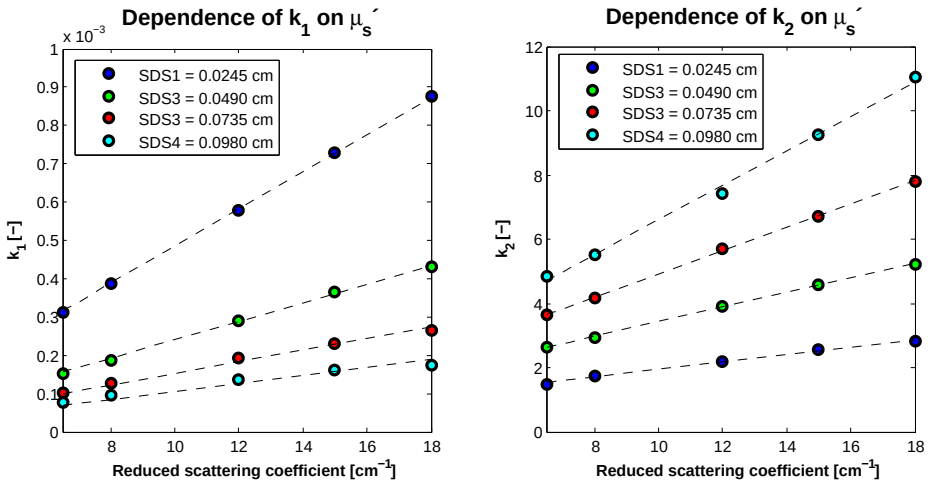

Figure 3.6: Dependence of parameters k_1 and k_2 on reduced scattering coefficient.

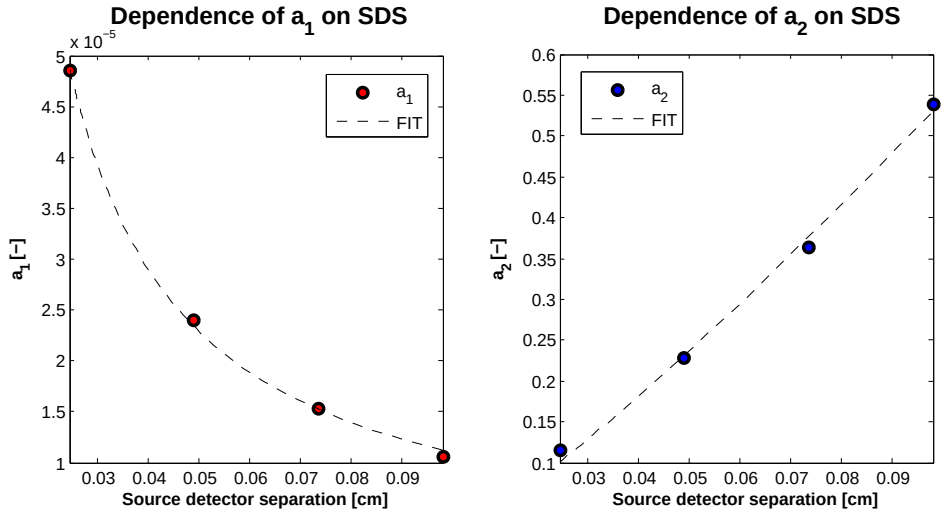

Figure 3.7: Dependence of parameters a_1 and a_2 on source detector separation.

The dependence can be expressed as:

$$a_1(r) = b_1 r^{c_1} \tag{3.16}$$
$$a_2(r) = c_2 r^{d_2} \tag{3.17}$$
$$b_2 = const \tag{3.18}$$

With these equations we can rewrite the equations for k_1 and k_2:

$$k_1 = b_1 r^{c_1} \mu_s' \tag{3.19}$$
$$k_2 = c_2 r^{d_2} \mu_s' + b_2 \tag{3.20}$$

And finally we can rewrite the main fitting equation as:

$$R_d(r) = \frac{b_1 r^{c_1} \mu_s'}{1 + (c_2 r^{d_2} \mu_s' + b_2) \frac{\mu_a}{\mu_s'}}. \tag{3.21}$$

This is our final empirical model, which should be more accurate than model defined by Equation 3.13.

3.2.4 Determination of the optical properties

After verification of basic model behavior we can proceed in determination of tissue optical properties. We will firstly compare models accuracy with the results from Zonios *et al.* [71]. After that we will test model for determination both reduced scattering and absorption coefficient. From calibration we obtain values for parameters for both model:

a_1	a_2	b_2
$8.99 \cdot 10^5$	$5.46 \cdot 10^6$	1.97

Table 3.1: Model 1: values of parameters obtained from calibration

b_1	c_1	b_2	c_2	d_2
$9.63 \cdot 10^{-7}$	-1.06	1.10	8.55	1.20

Table 3.2: Model 2: values of parameters obtained from calibration

Set of calibration data is different from data set used determination. Simulation for calibration is performed for four different values of absorption coefficient $[0, 2, 4, 6]$ and five values of reduced scattering coefficient $[6.5, 8, 12, 15, 18]$. We choose the same detector separation as will be used for experiment, parameters are in Table 4.1. All simulation were performed for 10^6 photons.

We test model ability of determination of absorption or reduced scattering coefficient while second one is fixed. For this method we use two-step fitting procedure. Firstly we determine values of absorption coefficient with reduced scattering coefficient as independent value. Second step is the same, we only change absorption coefficient for reduced scattering coefficient and conversely.

Program run is very fast and determination of both coefficient takes only seconds. Error in determination is calculated as:

$$Error = \frac{|value_{actual} - value_{estimated}|}{value_{actual}} \cdot 100\%. \tag{3.22}$$

Errors are calculated for each source-detector separation independently. From Tables on page 48 we can see that the model is very accurate for determination the value of reduced scattering coefficient. Overall error for reduced scattering coefficient is 3.70% and for absorption coefficient 9.23%. The second model

		Absorption coefficient $[cm^{-1}]$		
		0.5	1	4
SDS $[cm]$	0.0245	3.91	11.14	15.93
	0.0490	13.94	16.43	11.22
	0.0735	4.93	5.20	0.37

		Reduced scattering coefficient $[cm^{-1}]$				
		5	8	12	16	20
SDS $[cm]$	0.0245	3.91	3.25	1.09	2.31	4.41
	0.0490	7.52	1.86	3.48	4.26	4.63
	0.0735	3.14	3.17	6.08	2.60	3.81

Table 3.3: Model 1: Errors in percent. Upper table corresponds to errors for absorption coefficient, lower for reduced scattering coefficient.

		Absorption coefficient $[cm^{-1}]$		
		0.5	1	4
SDS $[cm]$	0.0245	0.52	8.80	14.34
	0.0490	1.90	3.27	1.06
	0.0735	5.93	0.78	7.94

		Reduced scattering coefficient $[cm^{-1}]$				
		5	8	12	16	20
SDS $[cm]$	0.0245	6.74	1.66	0.15	1.36	2.09
	0.0490	1.14	0.72	1.23	0.36	0.30
	0.0735	3.69	5.40	5.54	0.92	5.96

Table 3.4: Model 1: Errors in percent. Upper table corresponds to errors for absorption coefficient, lower for reduced scattering coefficient.

is tested in the same way and results are in Tables on page 48. Average error

for μ_s' is 4.95% and for μ_a 2.48%. The second model describes data better than the first model, it is also because it includes more parameters.

3.2.4.1 Simultaneous determination

But for better model validation, we need to test it in measurement of both coefficient simultaneously. Empirical models are described in previous section 3.2.3 and represent non-complicated and straightforward approximation. Coefficient determination is done by fitting diffuse reflectance data to Equations 3.13 and 3.21. Similar fitting procedure usually requires high number of fitting points or often whole spectrum (for example spectrally constrained measurement). We are testing minimalistic approach and therefore only four distances are used. This can reduce the accuracy but for some application it can be very advantageous. First model has errors 24.45% for absorption coefficient and 6.38% for reduced scattering coefficient. Second model has errors 38.02% for absorption coefficient and 10.04% for reduced scattering coefficient. But the higher errors are caused by very inaccurate determination for $\mu_a = 4cm^{-1}$ and $\mu_s' = 5cm^{-1}$ - over 100%. The average errors for other values are 28.32% for absorption coefficient and 5.75% for reduced scattering coefficient.

CHAPTER 4

Simulation and experiment

Model development is described in previous chapter and results from Monte Carlo simulation confirm model validity. We need to test model performance on the tissue simulation phantoms. Experiment was performed in the Dr. Quan Liu's lab at the Nanyang Technological University [49].

4.1 Tissue simulating phantoms

In this section we will describe more details about tissue simulating phantoms. These phantoms are very useful for validation of methods used for measuring tissue optical properties. They are also used for testing therapeutic methods and optimizing signal to noise ratio. Basic requirements are accurate description of scattering and absorbing properties and consistence over time. They can be fabricated from various materials. The most useful are hybrid phantoms allowing more types of measurement (elastic, biochemical or thermal) together with optical properties determination [46]. Requirements on phantom differ accordingly to the various applications. Precisely described optical properties and easy manufacturing are important for method validation. On the other hand phantoms for interlaboratory comparison need to be very stable over time. These requirements on phantoms are the most important for our application:

1. inexpensive and easy to manufacture
2. homogeneous in entire volume
3. precise characterization of optical properties
4. index of refraction have similar to the real tissue ($n = 1.4$)

To achieve both type of light interaction, tissue simulating phantoms are made as mixture of absorbers and scatterers. Intralipid, nutralipid, liposyn and microspheres are mainly used scatterers. Biological stain as trypan blue, molecular dyes, ink and hemoglobin are used as absorbers. Phantoms can be both solid and liquid. Liquid phantoms are easy to prepare and optical properties can be changed simply by increasing concentration of scatterers and absorbers. On the other hand, solid phantoms are more permanent and stable, as materials are used polymers, silicone or gelatin. It is also possible to fabricate multilayered phantoms for more complex modeling (for example for skin models)[46, 60].

4.1.1 Scattering properties

In the experiment we were using two different scatterers. Mainly monodisperse polystyrene microspheres Polybead® Microspheres with $1.00\mu m$ mean diameter was used. For experiment was available 2.5% solids (w/v) aqueous suspension. It is described in mass of particles in grams in milliliter of suspension denoted $W[g/ml]$. All specifications are described on the producers website [47]. Final values of reduced scattering coefficient for the experiment should be $5 - 25\ cm^{-1}$. In total we prepared six phantoms with different concentrations. To relate W and the scattering coefficient we need firstly calculate number density $ND[1/\mu m^{-3}]$, which describes number of particles in a given volume:

$$ND = \frac{6 \cdot W}{p \cdot \pi \cdot \ Diam^3}, \tag{4.1}$$

where p is density of polymer in grams per milliliter and $Diam$ is mean diameter of microspheres. Using Equation 4.1 we can calculate number density for given value of W. Then with known parameters as number density, refractive indexes of microspheres and surrounding medium and microsphere diameter we convert scattering efficiency to the scattering coefficient. For measurement in large volumes we were using 20% solution of Intralipid. This measurement was used in the first stage of experiment. Scattering properties were described by Staveren *et al.* [61]. Properties of the Intralipid were checked in articles from Ninni *et al.*[40] and Michels *et al.* [39]. Both agreed with the model used in the first paper and spectrum is shown in Figure 4.2.

4.1.2 Absorption properties

As absorbers we used hemoglobin solution with well known spectra for absorption coefficient from previous measurements in this lab. For experiment we need values of absorption coefficient between 0.5 to 4 cm-1. For this range maximum concentration $4mg/ml$ was mixed. Final spectrum is shown in Figure 4.3 for concentration $1mg/ml$.

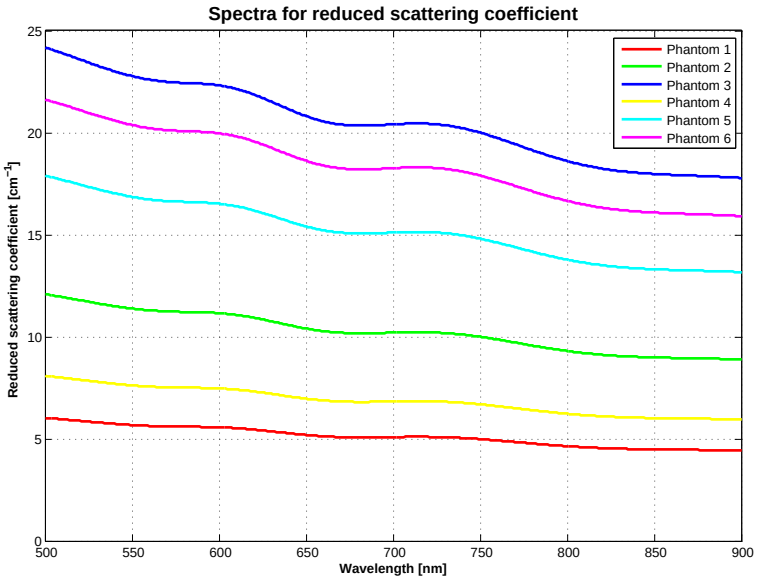

Figure 4.1: Scattering spectrum of Polybead® Microspheres with mean diameter $1.00\mu m$

4.1.3 Phantom preparation and measurement

For experiment we need diffuse reflectance data for several variations of absorption and reduced scattering coefficient. To achieve required values of optical coefficients, we need mix scatterers and absorbers into solution with PBS (Phospate Buffered Saline, pH 7.2). Relation of absorbers and scatterers concentration with concentration is discussed above. We tested several possibilities of reflectance data acquirement. First, we used relative values of reflectance. But for the later measurement it was not sufficient and we used absolute reflectance from phantoms. In this case the intensity of the light source has to be constant for all measurement (we have also counted with decreasing intensity of the source in long lasting measurements).

4.2 Instrumentation

Probe geometry is shown in Figure 4.4, it is composed of four detection fiber around one central illumination fiber. Refractive index of illumination fiber is 1.47, diameter of the fibers is 0.1mm. Distances of four channels from the illumination fiber (center-to-center distance) are: 0.245, 0.49, 0.735, 0.98 mm. Numerical aperture is 0.22. Probe specification is summarized in Table 4.1. The broadband source with strongest signal from 500 to $900nm$ was used for illumination . We have detected complete spectrum for diffuse reflectance but only one wavelength was chosen for determination.

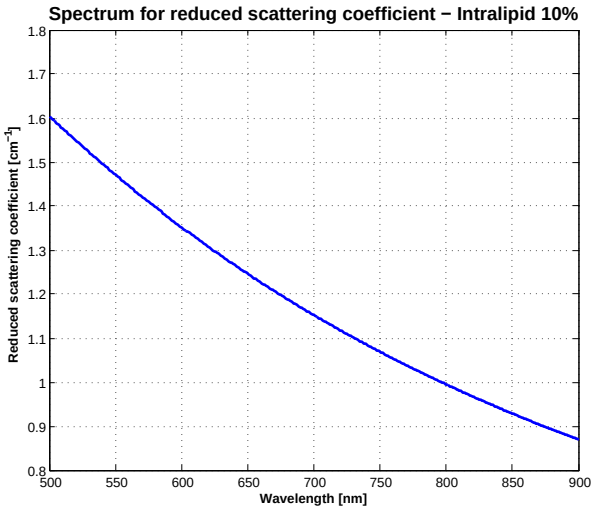

Figure 4.2: Scattering spectrum of Intralipid 10%

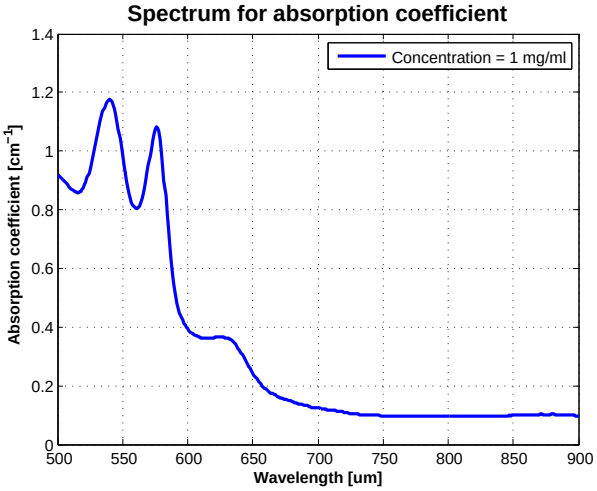

Figure 4.3: Absorption spectrum of hemoglobin

4.3 Experiment design

Final data for determination were measured in two separate experiments. We prepared three phantoms in each with different concentration of scatterers (in first experiment Phantoms 1-3, in second Phantoms 4-6). Unfortunately data obtained from Phantom 3 were very inaccurate and we had to exclude them. Firstly we measured diffuse reflectance with no added absorbers. After that we added calculated amount of hemoglobin and measured diffuse reflectance again. We repeated this approach for three different concentrations. Due to

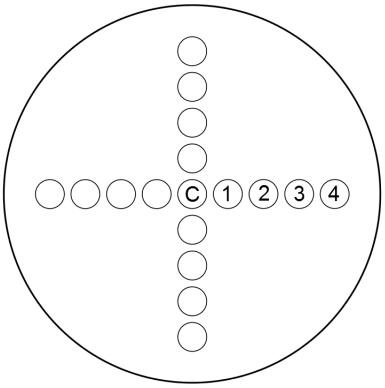

Figure 4.4: Probe geometry

Probe specification	
NA	0.22
Refractive index (illumination fiber)	1.47
Fibers diameter [mm]	0.1
Distance from the central fiber [mm]	
Channel 1	0.245
Channel 2	0.490
Channel 2	0.735
Channel 4	0.980

Table 4.1: Fiber probe parameters.

some problems with the probe we were not able to measure diffuse reflectance from the fourth channel and that was very limiting for later coefficient determination. Despite that we had still useful data and we could test our model. Before performing our algorithm, data were processed and we obtained set of measured diffuse reflectance data together with corresponding real values of absorption and reduced scattering coefficient. Source detector separations are described in Table 4.1. Experimental setup is shown in Figure 4.5.

4.3.1 Calibration

Calibration process was done in the same way as for Monte Carlo data. Final values of coefficients are in Tables 4.3.1, 4.3.1. Calibration process is computationally fast and needs to be performed only once for specific probe geometry.

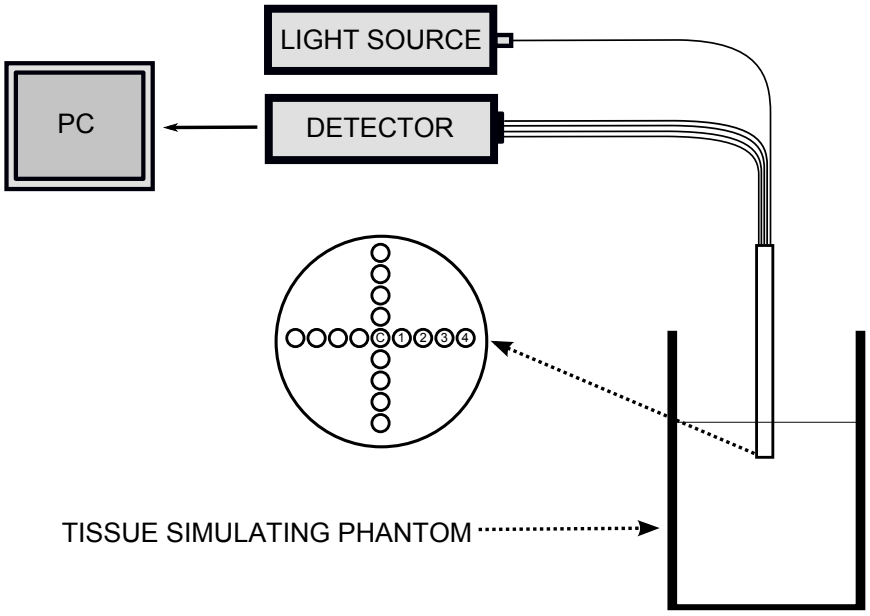

Figure 4.5: Experiment setup for spatially resolved diffuse reflectance measurement in tissue simulating phantoms.

a_1	a_2	b_2
$1.85 \cdot 10^{-1}$	$4.07 \cdot 10^{-1}$	1.51

Table 4.2: Model 1: values of parameters obtained from calibration.

b_1	c_1	b_2	c_2	d_2
7.62	$-8.94 \cdot 10^{-1}$	$-1.48 \cdot 10^{-1}$	2.67	$5.75 \cdot 10^{-1}$

Table 4.3: Model 2: values of parameters obtained from calibration.

4.4 The results of the experiment

As in previous section, we tested model performance for determination absorption and reduced scattering coefficient separately first. After that we performed simultaneous determination, but because of using only three measured distances the accuracy will be probably reduced.
First model shows average error 9.55% for absorption coefficient and 5.55% for reduced scattering coefficient, second model 6.45% for absorption coefficient

		Absorption coefficient $[cm^{-1}]$		
		1.04	1.87	4.17
SDS $[cm]$	0.0245	3.53	16.23	16.38
	0.0490	14.87	15.05	14.45
	0.0735	2.52	1.83	1.04

		Reduced scattering coefficient $[cm^{-1}]$				
		5.81	7.80	17.24	20.84	23.29
SDS $[cm]$	0.0245	8.77	4.61	0.84	8.54	8.19
	0.0490	10.26	7.86	0.98	11.64	10.01
	0.0735	2.72	0.41	3.82	2.40	2.25

Table 4.4: Model 1: Errors in percent. Upper table corresponds to errors for absorption coefficient, lower for reduced scattering coefficient.

		Absorption coefficient $[cm^{-1}]$		
		1.04	1.87	4.17
SDS $[cm]$	0.0245	23.57	4.83	10.76
	0.0490	4.16	2.60	6.48
	0.0735	0.54	0.80	3.41

		Reduced scattering coefficient $[cm^{-1}]$				
		5.81	7.80	17.24	20.84	23.29
SDS $[cm]$	0.0245	14.34	9.96	5.67	3.36	3.07
	0.0490	16.81	14.34	5.58	4.45	2.99
	0.0735	4.17	1.65	2.89	1.54	3.07

Table 4.5: Model 1: Errors in percent. Upper table corresponds to errors for absorption coefficient, lower for reduced scattering coefficient.

and 6.26% for reduced scattering coefficient. These errors are slightly higher than determination for Monte Carlo data.

4.4.1 Simultaneous determination

But both models in simultaneous determination show relatively high errors - model 1: 51.04% for μ_a and 22.30% for μ_s', model 2: 52.50% for μ_a and 26.30% for μ_s'. This may be caused by a combination of several factors but mostly due to using only three different distances in final fitting procedure. Measurement inaccuracy also contributed to the overall errors. We were working with very small phantoms and concentrations were therefore small as well. And even very small difference from calculated concentration can cause inac-

curacy. Errors for absorption coefficient are also higher because models often determine $\mu_a = 0$ for small coefficient values. Nevertheless, due to the minimalist approach, our model fits the data from the measurements quite well. Models were also relatively accurate for determination of reduced scattering coefficient for medium with zero or minimal absorption.

Conclusion

Measurement of tissue optical properties is an important topic in the field of biomedical optic. This thesis describes underlying theory of this topic and gives comprehensive overview of commonly used methods for determination of absorption and reduced scattering coefficient. Also, research in latest trends and demands on the measurement for therapeutic and diagnostic applications was conducted.

Main goal was to design fast and non-complicated method applicable for measurement in small volumes. Spatially resolved diffuse reflectance was chosen from various possibilities of measurement. Very often used models based on diffusion approximation are relatively complicated and are invalid in distances close to the source. Therefore empirical model was developed with the emphasis on clarity and simplicity. It is originally based on the model used for spectrally constrained measurement and it was modified for spatially resolved measurement.

First, the empirical model was tested on data from Monte Carlo simulation. Model was tested for both coefficients separately using two-step fitting procedure. Average errors for first model are 9.2% for μ_a and 3.7% for μ_s'. Errors for second model are 5.0% for μ_a and 2.5% for μ_s'. Modification for spatially resolved measurement was done through model parameters by expressing their dependence on the distance of the detector from illumination fiber. First model determines optical properties with average error 24.4% for μ_a and 6.4% for μ_s', second model shows errors 28.3% for μ_a and 5.8% for μ_s'. Final errors from Monte Carlo simulation are relatively small for such minimalistic approach.

Afterwards, an experiment on tissue simulating phantoms was performed. Due to some difficulties during the experiment, fourth detection fiber was not employed in measurement. That led to data reduction and limited us in more accurate determination. The same calculation of errors as for simulated data was applied on the obtained experimental data. For separate determination first model shows average errors 9.6% for μ_a and 5.6% for μ_s', second model 6.4% for μ_a and 6.3% for μ_s'. Simultaneous determination shows greater errors: for the first model an average errors are 51.0% for μ_a and 22.3% for μ_s', for second model 52.5% for μ_a and 26.3% for μ_s'.

Nevertheless, this method can be further developed and it was shown that spatially resolved measurement can be used even for very small distances from the source. In comparison to other methods, it is relatively simple and fast. Additionally, it does not demand expensive instrumental equipment.

Bibliography

[1] Bargo, P. R.; Prahl, S. A.; Goodell, T. T.; etc.: In vivo determination of optical properties of normal and tumor tissue with white light reflectance and an empirical light transport model during endoscopy. *Journal of Biomedical Optics*, volume 10, no. 3, 2005: pp. 034018–034018–15, doi:10.1117/1.1921907. Available at WWW: <http://dx.doi.org/10.1117/1.1921907>

[2] Beek, J. F.; Blokland, P.; Posthumus, P.; etc.: In vitro double-integrating-sphere optical properties of tissues between 630 and 1064 nm. *Physics in Medicine and Biology*, volume 42, no. 11, 1997: p. 2255. Available at WWW: <http://stacks.iop.org/0031-9155/42/i=11/a=017>

[3] Bevilacqua, F.; Berger, A. J.; Cerussi, A. E.; etc.: Broadband Absorption Spectroscopy in Turbid Media by Combined Frequency-Domain and Steady-State Methods. *Appl. Opt.*, volume 39, no. 34, Dec 2000: pp. 6498–6507, doi:10.1364/AO.39.006498. Available at WWW: <http://ao.osa.org/abstract.cfm?URI=ao-39-34-6498>

[4] Bevilacqua, F.; Piguet, D.; Marquet, P.; etc.: In Vivo Local Determination of Tissue Optical Properties: Applications to Human Brain. *Appl. Opt.*, volume 38, no. 22, Aug 1999: pp. 4939–4950, doi:10.1364/AO.38.004939. Available at WWW: <http://ao.osa.org/abstract.cfm?URI=ao-38-22-4939>

[5] Boas, D. A.; Pitris, C.; Ramanujam, N.: *Handbook of biomedical optics / edited by David A. Boas, Constantinos Pitris, Nimmi Ramanujam.* Boca Raton, FL : CRC Press, c2011., 2011, ISBN 1420090372.

[6] Branco, G.: *The development and evaluation of head probes for optical imaging if the infant head.* Dissertation thesis, Department of Medical Physics and Bioengineering, University College London, 2007.

[7] Calabro, K. W.; Aizenberg, E.; Bigio, I. J.: Improved empirical models for extraction of tissue optical properties from reflectance spectra. 2012: pp. 82300H–82300H–7, doi:10.1117/12.906753. Available at WWW: <http://dx.doi.org/10.1117/12.906753>

[8] Cheng-Lun Tsai, W.-J. W., Ji-Chung Chen: Near-infrared Absorption Property of Biological Soft Tissue Constituents. *Journal of Medical and Biological Engineering*, volume 21, no. 1, 2001.

[9] Cheong, W.-F.; Prahl, S.; Welch, A.: A review of the optical properties of biological tissues. *Quantum Electronics, IEEE Journal of*, volume 26, no. 12, Dec: pp. 2166–2185, ISSN 0018-9197, doi:10.1109/3.64354.

[10] Chernomordik, V. V.; Hattery, D. W.; Grosenick, D.; etc.: Quantification of optical properties of a breast tumor using random walk theory. *Journal of Biomedical Optics*, volume 7, Jan. 2002: pp. 80–87, doi:10.1117/1.1427049.

[11] Chin, L.; Pop, M.; Whelan, W.; etc.: Optical method using fluence or radiance measurements to monitor thermal therapy. *Review of Scientific Instruments*, volume 74, no. 1, 2003: pp. 393–395, ISSN 0034-6748, doi:10.1063/1.1519681.

[12] Dam, J. S.: *Optical analysis of biological media - continuous wave techniques*. Dissertation thesis, Department of Physics, Lund Institute of technology, 2000.

[13] Dam, J. S.; Andersen, P. E.; Dalgaard, T.; etc.: Determination of Tissue Optical Properties from Diffuse Reflectance Profiles by Multivariate Calibration. *Appl. Opt.*, volume 37, no. 4, Feb 1998: pp. 772–778, doi:10.1364/AO.37.000772. Available at WWW: <http://ao.osa.org/abstract.cfm?URI=ao-37-4-772>

[14] Dam, J. S.; Dalgaard, T.; Fabricius, P. E.; etc.: Multiple Polynomial Regression Method For Determination of Biomedical Optical Properties From Integrating Sphere Measurements. *Appl. Opt.*, volume 39, no. 7, Mar 2000: pp. 1202–1209, doi:10.1364/AO.39.001202. Available at WWW: <http://ao.osa.org/abstract.cfm?URI=ao-39-7-1202>

[15] Dam, J. S.; Pedersen, C. B.; Dalgaard, T.; etc.: Fiber-optic probe for noninvasive real-time determination of tissue optical properties at multiple wavelengths. *Appl. Opt.*, volume 40, no. 7, Mar 2001: pp. 1155–1164, doi:10.1364/AO.40.001155. Available at WWW: <http://ao.osa.org/abstract.cfm?URI=ao-40-7-1155>

[16] Dimofte, A.; Finlay, J. C.; Zhu, T. C.: A method for determination of the absorption and scattering properties interstitially in turbid media. *Physics in Medicine and Biology*, volume 50, no. 10, 2005: p. 2291. Available at WWW: <http://stacks.iop.org/0031-9155/50/i=10/a=008>

[17] Fantini, S.; Franceschini, M.-A.; Maier, J. S.; etc.: Frequency-domain multichannel optical detector for noninvasive tissue spectroscopy and oximetry. *Optical Engineering*, volume 34, no. 1,

1995: pp. 32–42, doi:10.1117/12.183988. Available at WWW: <http://dx.doi.org/10.1117/12.183988>

[18] Farrell, T. J.; Patterson, M. S.: A diffusion theory model of spatially resolved, steady-state diffuse reflectance for the noninvasive determination of tissue optical properties in vivo. *Med. Phys.*, volume 19, no. 4, 1992: pp. 879–888, doi:10.1109/PROC.1977.10612.

[19] Fishkin, J. B.; Coquoz, O.; Anderson, E. R.; etc.: Frequency-domain photon migration measurements of normal and malignant tissue optical properties in a human subject. *Appl. Opt.*, volume 36, no. 1, Jan 1997: pp. 10–20, doi:10.1364/AO.36.000010. Available at WWW: <http://ao.osa.org/abstract.cfm?URI=ao-36-1-10>

[20] Florian E. W. Schmidt, M.: *Development of a Time-Resolved Optical Tomography System for Neonatal Brain Imaging*. Dissertation thesis, Department of Medical Physics and Bioengineering, University College London, 1999.

[21] Grossweiner, L. I.; Rogers, B. H. G.; Grossweiner, J. B.; etc.: *The Science of Phototherapy: An Introduction / by Leonard I. Grossweiner, James B. Grossweiner, B.H. Gerald Rogers ; edited by Linda R. Jones.* Dordrecht : Springer, 2005., 2005, ISBN 9781402028854.

[22] Hale, G. M.; Querry, M. R.: Optical Constants of Water in the 200-nm to 200-μm Wavelength Region. *Appl. Opt.*, volume 12, no. 3, Mar 1973: pp. 555–563, doi:10.1364/AO.12.000555. Available at WWW: <http://ao.osa.org/abstract.cfm?URI=ao-12-3-555>

[23] Haskell, R. C.; Svaasand, L. O.; Tsay, T.-T.; etc.: Boundary conditions for the diffusion equation in radiative transfer. *J. Opt. Soc. Am. A*, volume 11, no. 10, Oct 1994: pp. 2727–2741, doi:10.1364/JOSAA.11.002727. Available at WWW: <http://josaa.osa.org/abstract.cfm?URI=josaa-11-10-2727>

[24] Hayakawa, C. K.; Hill, B. Y.; You, J. S.; etc.: Use of the δ-P1 Approximation for Recovery of Optical Absorption, Scattering, and Asymmetry Coefficients in Turbid Media. *Appl. Opt.*, volume 43, no. 24, Aug 2004: pp. 4677–4684, doi:10.1364/AO.43.004677. Available at WWW: <http://ao.osa.org/abstract.cfm?URI=ao-43-24-4677>

[25] Hetzel, F.; Patterson, M.; Preuss, L.; etc.: Recommended nomenclature for physical quantities in medical applications of light. *American Association of Physicists in Medicine. General Medical Physics Committee.*, 1996.

[26] Hull, E. L.; Foster, T. H.: Steady-state reflectance spectroscopy in the P3 approximation. *J. Opt. Soc. Am. A*, volume 18, no. 3, Mar 2001: pp. 584–599, doi:10.1364/JOSAA.18.000584. Available at WWW: <http://josaa.osa.org/abstract.cfm?URI=josaa-18-3-584>

[27] Ishimaru, A.: Theory and application of wave propagation and scattering in random media. *Proceedings of the IEEE*, volume 65, no. 7, July: pp. 1030–1061, ISSN 0018-9219, doi:10.1109/PROC.1977.10612.

[28] Johns, M.; Giller, C.; German, D.; etc.: Determination of reduced scattering coefficient of biological tissue from a needle-like probe. *Opt. Express*, volume 13, no. 13, Jun 2005: pp. 4828–4842, doi:10.1364/OPEX.13.004828. Available at WWW: <http://www.opticsexpress.org/abstract.cfm?URI=oe-13-13-4828>

[29] Kienle, A.; Glanzmann, T.: In vivo determination of the optical properties of muscle with time-resolved reflectance using a layered model. *Physics in Medicine and Biology*, volume 44, no. 11, 1999: p. 2689. Available at WWW: <http://stacks.iop.org/0031-9155/44/i=11/a=301>

[30] Kienle, A.; Lilge, L.; Patterson, M. S.; etc.: Spatially resolved absolute diffuse reflectance measurements for noninvasive determination of the optical scattering and absorption coefficients of biological tissue. *Appl. Opt.*, volume 35, no. 13, May 1996: pp. 2304–2314, doi:10.1364/AO.35.002304. Available at WWW: <http://ao.osa.org/abstract.cfm?URI=ao-35-13-2304>

[31] Kienle, A.; Patterson, M. S.: Determination of the optical properties of turbid media from a single Monte Carlo simulation. *Physics in Medicine and Biology*, volume 41, no. 10, 1996: p. 2221. Available at WWW: <http://stacks.iop.org/0031-9155/41/i=10/a=026>

[32] Kienle, A.; Patterson, M. S.; Dögnitz, N.; etc.: Noninvasive Determination of the Optical Properties of Two-Layered Turbid Media. *Appl. Opt.*, volume 37, no. 4, Feb 1998: pp. 779–791, doi:10.1364/AO.37.000779. Available at WWW: <http://ao.osa.org/abstract.cfm?URI=ao-37-4-779>

[33] KUBELKA, P.: New Contributions to the Optics of Intensely Light-Scattering Materials. Part I. *J. Opt. Soc. Am.*, volume 38, no. 5, May 1948: pp. 448–448, doi:10.1364/JOSA.38.000448. Available at WWW: <http://www.opticsinfobase.org/abstract.cfm?URI=josa-38-5-448>

[34] L.-H. Wang, S. J.; Zheng, L.-Q.: MCML - Monte Carlo modeling of light transport in multi-layered tissues. *Computer Methods and Programs in Biomedicine*, , no. 47, 1995: pp. 131–146.

[35] Lin, S.-P.; Wang, L.; Jacques, S. L.; etc.: Measurement of tissue optical properties by the use of oblique-incidence optical fiber reflectometry. *Appl. Opt.*, volume 36, no. 1, Jan 1997: pp. 136–143, doi:10.1364/AO.36.000136. Available at WWW: <http://ao.osa.org/abstract.cfm?URI=ao-36-1-136>

[36] Liu, Q.; Zhu, C.; Ramanujam, N.: Experimental validation of Monte Carlo modeling of fluorescence in tissues in the UV-visible spectrum. *Journal of Biomedical Optics*, volume 8, no. 2, 2003: pp. 223–236, doi:10.1117/1.1559057. Available at WWW: <http://dx.doi.org/10.1117/1.1559057>

[37] Martelli, F.; Sassaroli, A.; Del Bianco, S.; etc.: Solution of the time-dependent diffusion equation for layered diffusive media by the eigenfunction method. *Phys. Rev. E*, volume 67, May 2003: p. 056623, doi:10.1103/PhysRevE.67.056623. Available at WWW: <http://link.aps.org/doi/10.1103/PhysRevE.67.056623>

[38] Matcher, S. J.; Cope, M.; Delpy, D. T.: Use of the water absorption spectrum to quantify tissue chromophore concentration changes in near-infrared spectroscopy. *Physics in Medicine and Biology*, volume 39, no. 1, 1994: p. 177. Available at WWW: <http://stacks.iop.org/0031-9155/39/i=1/a=011>

[39] Michels, R.; Foschum, F.; Kienle, A.: Optical properties of fat emulsions. *Opt. Express*, volume 16, no. 8, Apr 2008: pp. 5907–5925, doi:10.1364/OE.16.005907. Available at WWW: <http://www.opticsexpress.org/abstract.cfm?URI=oe-16-8-5907>

[40] Ninni, P. D.; Martelli, F.; Zaccanti, G.: Intralipid: towards a diffusive reference standard for optical tissue phantoms. *Physics in Medicine and Biology*, volume 56, no. 2, 2011: p. N21. Available at WWW: <http://stacks.iop.org/0031-9155/56/i=2/a=N01>

[41] Nurse, J.; Sinclair, J.: *Electrical Engineering and Applied Computing*. Lecture Notes in Electrical Engineering, Springer, 2011, ISBN 9400711913.

[42] Palmer, G. M.; Ramanujam, N.: Monte Carlo-based inverse model for calculating tissue optical properties. Part I: Theory and validation on synthetic phantoms. *Appl. Opt.*, volume 45, no. 5, Feb 2006: pp. 1062–1071, doi:10.1364/AO.45.001062. Available at WWW: <http://ao.osa.org/abstract.cfm?URI=ao-45-5-1062>

[43] Patterson, M.; Madsen, S.; Moulton, J.; etc.: Diffusion equation representation of photon migration in tissue. In *Microwave Symposium Digest,*

1991., IEEE MTT-S International, 1991, ISSN 0149-645X, pp. 905–908 vol.2, doi:10.1109/MWSYM.1991.147155.

[44] Patterson, M. S.; Chance, B.; Wilson, B. C.: Time resolved reflectance and transmittance for the non-invasive measurement of tissue optical properties. *Appl. Opt.*, volume 28, no. 12, Jun 1989: pp. 2331–2336, doi:10.1364/AO.28.002331. Available at WWW: <http://ao.osa.org/abstract.cfm?URI=ao-28-12-2331>

[45] Pickering, J. W.; Prahl, S. A.; van Wieringen, N.; etc.: Double-integrating-sphere system for measuring the optical properties of tissue. *Appl. Opt.*, volume 32, no. 4, Feb 1993: pp. 399–410, doi:10.1364/AO.32.000399. Available at WWW: <http://ao.osa.org/abstract.cfm?URI=ao-32-4-399>

[46] Pogue, B. W.; Patterson, M. S.: Review of tissue simulating phantoms for optical spectroscopy, imaging and dosimetry. *Journal of Biomedical Optics*, volume 11, no. 4, July 2006: pp. 041102–16. Available at WWW: <http://link.aip.org/link/?JBO/11/041102/1>

[47] Polysciences, I.: Description of used scatterers. 2013. Available at WWW: <http://www.polysciences.com/>

[48] Prahl, S. A.; van Gemert, M. J. C.; Welch, A. J.: Determining the optical properties of turbid mediaby using the adding–doubling method. *Appl. Opt.*, volume 32, no. 4, Feb 1993: pp. 559–568, doi:10.1364/AO.32.000559. Available at WWW: <http://ao.osa.org/abstract.cfm?URI=ao-32-4-559>

[49] Quan, A. P. L.: Dr. Quan Liu's Lab. 2013. Available at WWW: <http://www.ntu.edu.sg/home/quanliu/>

[50] R. Weissleder, A. R., B.D. Ross; Gambhir, S.: *Molecular Imaging: Principles and Practice*, chapter 14: Diffuse Optical Tomography and Spectroscopy. Pmph-usa, 2010.

[51] Reif, R.; A'Amar, O.; Bigio, I. J.: Analytical model of light reflectance for extraction of the optical properties in small volumes of turbid media. *Appl. Opt.*, volume 46, no. 29, Oct 2007: pp. 7317–7328, doi:10.1364/AO.46.007317. Available at WWW: <http://ao.osa.org/abstract.cfm?URI=ao-46-29-7317>

[52] Ren, H.; Fang, Z.: Lattice random walk modeling of photon migration in turbid media. 1998: pp. 148–157, doi:10.1117/12.317859. Available at WWW: <http://dx.doi.org/10.1117/12.317859>

[53] S. A. Prahl, S. L. J.: Oregon Medical Laser Center. 2012. Available at WWW: <http://omlc.ogi.edu/>

[54] Simpson, C. R.; Kohl, M.; Essenpreis, M.; etc.: Near-infrared optical properties of ex vivo human skin and subcutaneous tissues measured using the Monte Carlo inversion technique. *Physics in Medicine and Biology*, volume 43, no. 9, 1998: p. 2465. Available at WWW: <http://stacks.iop.org/0031-9155/43/i=9/a=003>

[55] Svensson, T.; Swartling, J.; Taroni, P.; etc.: Characterization of normal breast tissue heterogeneity using time-resolved near-infrared spectroscopy. *Physics in Medicine and Biology*, volume 50, no. 11, 2005: p. 2559. Available at WWW: <http://stacks.iop.org/0031-9155/50/i=11/a=008>

[56] Svensson T, E. M.-S. K., Andersson-Engels S: *In vivo* optical characterization of human prostate tissue using near-infrared time-resolved spectroscopy. *Journal of Biomedical Optics*, volume 12, no. 1, Jan 2007. Available at WWW: <http://www.ncbi.nlm.nih.gov/pubmed/17343497>

[57] The MathWorks, I.: MathWorks®. 2013. Available at WWW: <http://www.mathworks.com/>

[58] Treweek, S.; Barbenel, J.: Direct measurement of the optical properties of human breast skin. *Medical and Biological Engineering and Computing*, volume 34, 1996: pp. 285–289, ISSN 0140-0118, doi:10.1007/BF02511239. Available at WWW: <http://dx.doi.org/10.1007/BF02511239>

[59] Tuchin, V. V. (editor): *Handbook of Optical Biomedical Diagnostics*, *Lecture Notes in Electrical Engineering*, volume PM107, chapter 7: Frequency-domain techniques for tissue spectroscopy and imaging. SPIE press., 2002, ISBN 9780819442383.

[60] Tuchin, V. V.: *Tissue optics: light scattering methods and instruments for medical diagnosis / Valery Tuchin.* SPIE Press monograph: PM166, Bellingham, Wash. : SPIE/International Society for Optical Engineering, c2007., 2007, ISBN 9780819464330.

[61] van Staveren, H. J.; Moes, C. J. M.; van Marle, J.; etc.: Light scattering in Intralipid-10 in the wavelength range of 400-1100 nm. *Applied Optics*, volume 30, Nov 1991: pp. 4507–4514, doi:10.1364/AO.30.004507.

[62] van Veen, R. L.; Sterenborg, H.; Pifferi, A.; etc.: Determination of VIS- NIR absorption coefficients of mammalian fat, with time- and spatially resolved diffuse reflectance and transmission spectroscopy. In *Biomedical Topical Meeting*, Optical Society of America, 2004, p. SF4. Available at WWW: <http://www.opticsinfobase.org/abstract.cfm?URI=BIO-2004-SF4>

[63] Wang, L. V.; Jacques, S. L.: Monte Carlo Modeling of Light Transport in Multi-layered Tissues in Standard C. *Program*, volume 10, 1992.

[64] Welch, A. J.; Gemert, M. J.: *Optical-Thermal Response of Laser-Irradiated Tissue / edited by Ashley J. Welch, Martin J.C. Gemert.* Dordrecht : Springer Science+Business Media B.V., 2011., 2011, ISBN 9789048188314.

[65] Wilson, B. C.; Patterson, M. S.; Flock, S. T.: INDIRECT VERSUS DIRECT TECHNIQUES FOR THE MEASUREMENT OF THE OPTICAL PROPERTIES OF TISSUES. *Photochemistry and Photobiology*, volume 46, no. 5, 1987: pp. 601–608, ISSN 1751-1097, doi:10.1111/j.1751-1097.1987.tb04820.x. Available at WWW: <http://dx.doi.org/10.1111/j.1751-1097.1987.tb04820.x>

[66] Wyman, D. R.; Patterson, M. S.; Wilson, B. C.: Similarity relations for the interaction parameters in radiation transport. *Appl. Opt.*, volume 28, no. 24, Dec 1989: pp. 5243–5249, doi:10.1364/AO.28.005243. Available at WWW: <http://ao.osa.org/abstract.cfm?URI=ao-28-24-5243>

[67] Yaqin, C.; Ling, L.; Gang, L.; etc.: Determination of tissue optical properties from spatially resolved relative diffuse reflectance by PCA-NN. In *Neural Networks and Signal Processing, 2003. Proceedings of the 2003 International Conference on*, volume 1, 2003, pp. 369–372 Vol.1, doi: 10.1109/ICNNSP.2003.1279286.

[68] van der Zee, P.: *Measurement and modelling of the optical properties of human tissue in the near infrared*. Dissertation thesis, Department of Medical Physics and Bioengineering, University College London, 1992.

[69] Zhang, L.; Wang, Z.; Zhou, M.: Determination of the optical coefficients of biological tissue by neural network. *Journal of Modern Optics*, volume 57, no. 13, 2010: pp. 1163–1170, doi:10.1080/09500340.2010.500106.

[70] Zonios, G.; Bassukas, I.; Dimou, A.: Comparative evaluation of two simple diffuse reflectance models for biological tissue applications. *Appl. Opt.*, volume 47, no. 27, Sep 2008: pp. 4965–4973, doi:10.1364/AO.47.004965. Available at WWW: <http://ao.osa.org/abstract.cfm?URI=ao-47-27-4965>

[71] Zonios, G.; Dimou, A.: Modeling diffuse reflectance from semi-infinite turbid media: application to the study of skin optical properties. *Opt. Express*, volume 14, no. 19, Sep 2006: pp. 8661–8674, doi:10.1364/OE.14.008661. Available at WWW: <http://www.opticsexpress.org/abstract.cfm?URI=oe-14-19-8661>

[72] Zonios, G.; Dimou, A.: Modeling diffuse reflectance from homogeneous semi-infinite turbid media for biological tissue applications: a Monte Carlo study. *Biomedical optics express*, volume 2, no. 12, 2011: pp. 3284–94.

[73] Zonios, G.; Perelman, L. T.; Backman, V.; etc.: Diffuse Reflectance Spectroscopy of Human Adenomatous Colon Polyps In Vivo. *Appl. Opt.*, volume 38, no. 31, Nov 1999: pp. 6628–6637, doi:10.1364/AO.38.006628. Available at WWW: <http://ao.osa.org/abstract.cfm?URI=ao-38-31-6628>

APPENDIX A

Content of CD

Thesis/	
MT_Hlavac.pdf	- the master thesis in PDF format
img/	- the figures used in thesis
*.pdf	- the figures in format PDF
*.png	- the figures in format PNG
MatlabCode/	
CodeDescription.txt	- the description of Matlab programme
ModelTesting/	
ModelBehaviour.m	- the basic model behaviour
Data/	- the data files from Monte Carlo simulation
ModelDevelopment/	
Model_1/	- the codes used for the first model development
Model_2/	- the codes used for the second model development
OpticalPropertiesDetermination/	
MC/	- the codes for Monte Carlo data
Phantoms/	- the codes for data from experiment

APPENDIX B

Typical values of tissue optical properties

Tissue	Wavelength [λ]	$\mu_a[mm^{-1}]$	$\mu'_s[mm^{-1}]$
Caucasian dermis	633	0.033 ± 0.009	2.73 ± 0.54
	700	0.019 ± 0.006	2.32 ± 0.41
	900	0.007 ± 0.006	1.63 ± 0.25
Negroid dermis	633	0.241 ± 0.153	3.21 ± 2.04
	700	0.149 ± 0.088	2.68 ± 1.41
	900	0.045 ± 0.018	1.81 ± 0.04
Subdermis	633	0.013 ± 0.005	1.26 ± 0.34
	700	0.009 ± 0.003	1.21 ± 0.32
	900	0.012 ± 0.004	1.08 ± 0.27
Muscle	633	0.121	0.89
	700	0.046	0.83
	900	0.032	0.59

Table B.1: Values of absorption and reduced scattering coefficient of the various tissue types [54].

Tissue	Wavelength [λ]	$\mu_a[mm^{-1}]$	$\mu'_s[mm^{-1}]$
Neonatal grey matter	650-990	0.04-0.08	0.4-0.9
Neonatal white matter	650-990	0.04-0.07	0.5-1.2
Adult brain	700-990	0.1-0.2	2-5
Adult grey matter	811	0.018-0.019	0.48-0.74
Adult grey matter	849	0.018-0.019	0.45-0.74
Adult grey matter	650-900	0.04-0.06	1.9-2.2
Adult white matter	849	0.013	0.98
Adult white matter	650-900	0.02-0.03	8-10
Adult skull	849	0.022	0.91

Table B.2: Values of absorption and reduced scattering coefficient of the brain tissue from different researchers [20].